Forschungszentrum Karlsruhe

Technik und Umwelt

Wissenschaftliche Berichte

FZKA 6604

Single rod quench tests with Zr-1Nb cladding. Comparison with Zircaloy-4 cladding tests and modelling

J. Stuckert, M. Steinbrück, U. Stegmaier

Institut für Materialforschung

Programm Nukleare Sicherheitsforschung

Forschungszentrum Karlsruhe GmbH, Karlsruhe
2001

Abstract

Nine separate-effects tests with VVER fuel rod simulators (Zr-1Nb cladding, 150 mm length) on the cooldown by steam in the temperature range 1100°C-1600°C have been performed. The main parameters of the tests were the degree of pre-oxidation and the rod temperature at the onset of cooldown. The tube specimens were pre-oxidised (100-300 µm oxide thickness) at 1400°C in a steam/argon gas mixture in the QUENCH rig before quenching. Then specimens were rapidly cooled down by steam (mass flow 1 g/s, temperature of about 150°C), which was injected into the test section simulating conditions above the quench-water front during core reflooding. The mechanical behaviour of the cladding tubes depends on the cooldown temperature and the extent of pre-oxidation. The formation of through-wall cracks was observed in the experiments with ZrO_2 layer thickness larger than 200 µm. The hydrogen release during pre-oxidation and quenching phases was analysed. Up to 1400°C no deviation of the hydrogen release rate from the analogous tests with Zircaloy-4 cladding was found. Additionally the amount of absorbed hydrogen in segments of Zr-1Nb test specimens was analysed after the tests. The results show that under the same conditions the Zr-1Nb cladding tubes absorb less hydrogen than the Zircaloy-4 ones.

Abschreckexperimente mit Zr-1Nb Hüllrohren.
Vergleich mit Zircaloy-4 Versuchen und Modellierung

Zusammenfassung

Neun Einzelstab-Versuche mit kurzen (150 mm) VVER Brennstabsimulatoren zum mechanischen Verhalten von Zr-1Nb-Hüllrohren während des Dampfabschreckens von Temperaturen zwischen 1100°C und 1600°C sind in der kleinen FZK QUENCH Anlage durchgeführt worden. Die Proben wurden bis zu Oxidschichtdicken von 300 µm voroxidiert und in Wasserdampf mit einer Rate von 1 g/s abgeschreckt. Makroskopische durchgehende Risse durch das Hüllrohr wurden beim Dampfabschrecken in den Experimenten mit Oxidschichtdicken größer als 200 µm gebildet. Die Wasserstofffreisetzung während der Tests mit Zr-1Nb-Stäben wurde mittels Massenspektrometer gemessen. Bis zur Temperatur von 1400°C ist die Oxidationskinetik von Zr-1Nb und Zircaloy-4 vergleichbar. Oberhalb 1400°C nimmt die Kinetik der Wasserstoffproduktion im Vergleich zu Zircaloy-4 stark zu. Die Menge des absorbierten Wasserstoffs in den Zr-1Nb-Proben wurde analysiert. Die Resultate zeigen, daß bei gleichen Bedingungen die Zr-1Nb-Hüllrohre weniger Wasserstoff absorbieren als Zircaloy-4 Rohre.

Content

List of Tables

List of Figures

1. Introduction

The injection of water to cool the degrading core down is an important accident management measure for controlling severe accident transients in the light water reactors. Reflooding of an uncovered core is the main measure of operator actions to prevent the melt down of the core. The phenomena under these conditions (complex heat transfer between cladding and water, formation of cracks in the oxidised cladding, hydrogen uptake and release during cladding oxidation) for rods with the Zircaloy-4 cladding have been studied within the QUENCH program at Forschungszentrum Karlsruhe [1,2]. However, in the last time a number of new corrosion-resistant cladding materials for light water reactors with increased burnup has been proposed. A promising variant is the duplex cladding tube with the outer layer made of Zr-Nb alloy. Besides that, such alloys are being used in Russian VVER and in Canadian CANDU reactors. Therefore, an extensive separate-effects experimental database is required for Zr-1Nb claddings as a basis for the improvement of existing computer models.

2. Test rig and experimental procedure

For the experiments with Zr-1Nb rods the same equipment as for experiments with Zircaloy-4 rods was used [1, 2]. The design of the QUENCH rig is shown in Fig. 1.

The specimen used in the tests was a segment of VVER fuel rod cladding tube with a length of 150 mm, an outer diameter 9.13 mm (for comparison: the outer diameter of Zircaloy-4 cladding tubes is 10.75 mm) and a wall thickness of 0.705 mm (for Zircaloy-4 tube: 0.725 mm). The specimen was filled with high density yttria stabilised ZrO_2 pellets with an outer diameter 7.55 mm and a height 11 mm to simulate the fuel pellets.

The specimen was suspended by a thin Zry capillary tube inside a quartz tube. Heating was provided by an induction coil around the section of the quartz tube. Power was supplied to the coil from a 20 kW generator, at a frequency of 700 kHz, which induced currents in the bulk of the metal with consequent Joule heating. The feedback regulation of generator was performed by means of a pyrometer, focused on the specimen surface at the centre of the rod. Temperature at the outer surface of the cladding was measured by thermocouples at three elevations: 30 mm, 75 mm and 120 mm. The Pt/Rh thermocouples were fixed at the outer pre-oxidised tube surface by a Pt/Rh wire.

Before the tests the specimens have been pre-oxidised to a small extent to prevent eutectic interactions between thermocouples and cladding surface. This thin oxide scale was also formed in the QUENCH rig by exposing specimens with temperature 1200°C in argon/oxygen atmosphere for one minute (Fig. 3). The resulting protection oxide layer thickness was 20 - 30 µm.

The scheme of the test conduct is presented in Fig. 2. The following phases for the test sequence can be distinguished. First, an initial phase, during which the facility was prepared for the actual test. The specimen was heated up to 1000°C under constant argon flow with the addition of 20% oxygen to prevent dissolution of the protection oxide layer. After establishing of the thermal equilibrium the steam was injected at a constant rate of 0.08 g/s. Second, during the enhanced pre-oxidation

period, the specimen was heated up to 1400°C under a constant flow of argon and steam through the test section. The specimen was kept at this temperature until the desired oxide layer thickness is reached. Finally, the specimen was heated or cooled to the desired initial temperature at the onset of cooldown. The test was completed by increasing the steam flow rate to 1 g/s (steam temperature about 150°C) and switching off the inductive heating.

The outcoming gas composition was measured by "Balzers GAM-300" mass spectrometer (MS). GAM-300 is a completely computer controlled quadrupole MS with 8 mm rod system which allows quantitative measurement of gas concentrations down to about 10 vppm. To avoid steam condensation the whole off-gas system was heated to about 150°C. During the whole test argon was supplied as carrier and reference gas for quantitative analysis. The main task of the MS was to measure the hydrogen release rate; additionally the concentrations of steam, oxygen and nitrogen were measured to control the process. Fig. 4 – Fig. 12 show the measured hydrogen generation rate and calculated integral hydrogen generation during the pre-oxidation and cooldown periods.

The amount of hydrogen absorbed by the specimens was analysed by hot extraction under flowing argon in the LAVA facility coupled with a mass spectrometer. 1 cm long tube segments from the bottom, centre and top parts of each specimen were analysed. The specimens were kept at 1400°C for ca. 15 min under a well defined argon gas flow. The hydrogen release was analysed by the GAM-300 mass spectrometer. Fig. 13 shows typical temperature curves and MS results for specimens with 19 min pre-oxidation and different cool-down temperatures, as an example.

After the tests detailed metallographical analysis of the cladding structures on the elevations, corresponding to the lower, middle and upper TC locations were performed. 1 cm long tube segments were embedded, ground, lapped and finally polished by means of STRUER's equipment. The microphotographs were taken by means of "Reichert-Jung" metallographical light microscope, coupled through the "SensiCam" 12-bit CCD-camera with the computer. The Software "analySIS" was applied for the measurements.

3. Experimental results

3.1. Chemical analysis

The chemical analysis for both as-received cladding materials was performed. The results are given as wt.% values in Table 1.

3.2. Temperature evolution

The thermocouple readings are depicted in Fig. 4 – Fig. 12. Because of the finite coil dimensions all specimens had non-uniform axial temperature profile with a maximum in the middle of the tube segment. The lowest temperatures were measured at the top of the tube. The difference between thermocouple values was up to 200 K. The injection of 1 g/s steam 30 s before power shut-off causes a temporary decrease of the specimen temperature in all the experiments performed. This temperature drop was soon compensated by automatically increased electrical heating.

Temperature excursions as observed in the CORA quench tests [4] and QUENCH bundle tests QU-02 and QU-03 [5] were not observed in any of the reported single rod tests. One reason for that is the high radiative heat loss in the small QUENCH rig. Nevertheless, a temperature deviation from the regular monotonically decreasing during the cooldown phase was detected in almost all Zircaloy-4 single rod tests [2] as well as in most tests with the Zr-1Nb cladding (exothermic deviations in Fig. 7 - Fig. 12). The same deviation was also registered by pyrometer during the formation of the insulating layer before all tests (Fig. 3).

These exothermic deviations from a regular cooldown curve are probably caused by the β->α phase transition in the base metal. Differential thermal analysis (DTA) tests with Zircaloy-4 and Zr-1Nb samples were performed to check this hypothesis (Fig. 14). The thermal effect at about 800°C is more pronounced for Zirconium-Niobium. The scattering of the onset of the temperature deviation in Fig. 7 – Fig.12 can be connected to different phase transition temperatures for the different oxygen and hydrogen contents in the metal phase due to different pre-oxidation times.

The DTA results were also used for the correction of pyrometer temperature reading during the thin protection oxide layer formation.

Some TCs during the tests showed erroneous values. Such significant deviations from the real temperature occurred, in particular, during the rapid increase of the generator power. This shows that TC errors are probably caused by the inductive heating. The TC readings always normalised after the generator power shut off and the cooldown phase was characterised by the adequate temperature measurements.

The temperature data obtained in this test series and shown in Fig. 4 – Fig.12 can be used for validation of SA codes, especially with respect to the quench phase.

3.3. Post-test non-destructive measurements

After the tests, photographs of each specimen were taken and non-destructive measurements of the following parameters were performed (Table 2): oxide layer thickness, weight gain, tube diameter increase, tube length increase. The weight gains correlate well with the tube diameter increase and can be interpreted as a result of oxidation (formation of α-Zr(O) and oxide layers) .

Fig. 15 – Fig. 16 show the appearance of specimens after the cooldown from different temperatures. The oxide layer thickness at the onset of the cooldown phase was between 150 and 550 µm. Some specimens were broken during handling. Nevertheless they are quite stable mechanically and show no indications of spalling of the oxide scale. The outer surface of the cladding tubes is mostly dark which can be seen in Fig. 17. Here, the comparison of Zircaloy and Zirconium-Niobium claddings after the cooldown tests under the same conditions shows that at least the optical properties of oxide layers on the Zry and Zirconium-Niobium surfaces are different. It means also that these surfaces have different emissivity coefficients. Fig. 18 illustrates the differences of the optical properties for both materials. The reflectivity of Zircaloy-4 tube surface is higher than reflectivity of Zr-1Nb tube surface at room temperature. The measurements were performed by means of a light spectrometer [6]. Analogous measurements are necessary for the temperatures up to Zirconium melting temperature in the infra-red wavelength range.

The crack pattern on the surface of the Zr-1Nb cladding tubes is not so pronounced and regular as for Zircaloy-4 tubes. For Zircaloy-4 the development of regular nets of longitudinal and circumferential through-wall cracks is typical [2], [3]. For Zr-1Nb tubes only some longitudinal through-wall cracks at 1100°C, 1200°C and 1400°C and a lot of short surface cracks were observed (Fig. 19). For the Zr-1Nb specimen with cooldown from 1600°C there are only short cracks in the oxide layer (Fig. 20).

3.4. Metallographic examination

After the tests a detailed metallographical analysis of the cladding cross-sections was performed at three elevations for each rod (Fig. 21 – Fig. 31). Three typical layers (oxide layer, brittle α-Zr(O) layer, ductile β-Zr layer) were identified and measured. The results of the thickness measurements are summarised in the Table 3.

Fig. 25 and Fig. 29 show that in contrast to the tests with Zircaloy-4 [2] the surfaces of the through-wall cracks in Zr-1Nb tubes are practically not oxidised.

The metallographical results for the specimen which was cooled down from ~1600°C are especially interesting. Fig. 31 shows the results of the metallographical analysis of the cladding cross-section from the middle of the rod. The local temperature on the surface at this elevation was slightly higher than 1700°C. There are no through-wall cracks at all. One can see only cracks in the outer surface oxide layer and cracks in the α-Zr(O) layer. There are no cracks in the inner part of the oxide layer (initially cubic phase). Contact with the pellet led to the oxidation of the internal surface of the cladding at the temperature near the Zirconium melting point.

The results of the metallographical analysis allow to draw the dependence of typical layer thickness on the pre-oxidation duration. In Fig. 32 the measurement results for the specimens, which were cooled down from 1200°C are presented. The local pre-oxidation temperatures were not always constant and varied from test to test. Nevertheless, a linear (for these large oxidation duration) regression dependence of layer thickness vs. pre-oxidation time for each elevation and for each type of layer acceptably fits the experimental data. The analysis shows that linear correlation of this experimental data is more precise than the parabolic one. The reason of such deviation from the parabolic law can be the formation of micro cracks and pores in the thick oxide layer.

Fig. 33 shows the correlation between the cladding oxygen content (calculated from the weight gain measurements) and the layers thickness. One can see, that for the same oxygen content the specimens have thicker α-Zr(O) layers, which were cooled down from the higher temperature. That shows the significant influence of the temperature history on the oxygen distribution in the cladding.

3.5. Hydrogen release and absorption

One of main tasks of these tests was the quantitative description of the hydrogen generation kinetics. Fig. 5 – Fig. 13 show the sharp increase of the hydrogen release during heat-up to 1400°C for all tests. The increase of the hydrogen generation for the test No. 4 (Fig. 13) during heat-up to 1600°C is much more pronounced. There is no noticeable increase of hydrogen generation during the quench phase for all the tests. The results of the hydrogen release measurements during the tests are summarised in Table 4.

Fig. 34 - Fig. 38 show the comparison of the hydrogen release between Zr-1Nb tests and corresponding Zircaloy-4 tests [2]. One can see that up to 1400°C the hydrogen

production rate for the Zircaloy-4 specimens is always somewhat higher. This difference can be due to greater axial temperature gradient in the tests with Zr-1Nb, than in the tests with Zircaloy-4 (the evidence for that is the greater oxide layer thickness gradient along a Zr-1Nb cladding, than along a Zircaloy-4 tubes – see Table 4) and due to the difference in the cladding surface areas because of the different tube radii. At the same time one can see that after the rate maximum is achieved the hydrogen production rate changes more quickly for Zircaloy-4 specimens than for Zr-1Nb specimens. Also, for both cases (Zr-1Nb and Zircaloy-4) the part of hydrogen that was generated during of the quench phase is small (<10%) in comparison to the hydrogen production during the pre-oxidation.

There are two possible sources of the hydrogen production during the quenching phase: 1) the metallic surface of the through-wall cracks, developed at the onset of cool-down and 2) the enhanced contact of the metallic layer with the steam owing to cracking of the oxide layer. Fig. 39 - Fig. 40 show a comparison of the oxide layer structures and through-wall cracks oxidation for the Zr-1Nb and Zircaloy-4. One can see, that in Zr-1Nb case the oxide layer is uniformly porous on the whole depth, while the oxide layer of Zircaloy-4 is mainly porous only on outer layer (outside the thin Sn-containing boundary layer). On the other hand, the surface of through-wall cracks of Zircaloy-4 specimen is more oxidised than the one of Zr-1Nb. Therefore the hydrogen production during the cool-down of Zircaloy-4 is more controlled by the oxidation of through-wall cracks (according to measured crack length the contribution of the oxide volume in the cracks is about 10% of the oxide volume at the cladding surface[2, 3]). In the case of Zr-1Nb hydrogen generation is mainly conditioned by the cracking of the oxide layer.

The test with cool-down from 1600°C is quite different from the tests with the cool-down from 1400°C and lower. The hydrogen production sharply increases at the onset of heating after the pre-oxidation phase in the test with Zr-1Nb specimen in comparison with Zircaloy-4 case. Furthermore, the hydrogen release on the cool-down for Zr-1Nb is 30% of the total hydrogen production during the test. But, for the Zircaloy-4 specimen this value is only ~10%. This is probably connected with more intensive formation of surface cracks in Zr-1Nb cladding than in Zircaloy-4 one. The oxidised surface of the Zircaloy-4 cladding is relatively smooth and there are only some longitudinal through-wall cracks [2]. The oxidised surface of Zr-1Nb cladding has a lot of short but relatively wide cracks (Fig. 20 and Fig. 31).

Table 5 summarises the results of the analysis of the hydrogen amount absorbed in the metal phases of the rods. The distribution of hydrogen along the axial direction is influenced by the temperature gradient along the rod. Nevertheless, one can see that in the similar conditions the Zr-1Nb cladding tubes absorb significantly less hydrogen than Zircaloy-4 ones.

3.6. SVECHA calculations

A detailed analysis of the process development during the pre-oxidation and cool-down phases was performed by post-test calculations with the SVECHA code [7] for some tests. Each specimen was divided into three longitudinal zones with axially uniform temperature. The SVECHA code was applied for each of this zones separately. In these simulations the induction power input was set up in such a way that tube surface temperature followed the experimentally measured one. An example of the corresponding calculation results for the test No. 9 (cool-down from 1100°C) is shown in Fig. 41-Fig. 43 and for the test No. 8 (cool-down from 1400°C) in Fig. 45-Fig. 47. For the calculation of the hydrogen production of the whole rod the

results from three zones were added up (Fig. 44 and Fig. 48). The analysis of the obtained results shows that SVECHA calculations agree qualitatively with Zr-1Nb experimental data but overestimate ZrO_2 and α-Zr(O) thicknesses as well as the hydrogen production rate. This can be explained by other kinetic parameters for Zr-1Nb (SVECHA code was validated only for Zircaloy-4 material). On the other hand there are not enough experimental data for the both materials in the temperature range between 1400°C and 1600°C.

Acknowledgements

The authors thank Dr. Ch. Adelhelm, Analytical Department of the Institute for Material Research I at FZK, for the conduct of the chemical analysis.

We are very grateful to Mr. G. Schanz, FZK, and Dr. A. Palagin, IBRAE Moscow, for the careful review of the manuscript.

4. Summary and Conclusions

- Nine separate-effects tests with fuel rod simulators on the mechanical behaviour of the Zr-1Nb cladding tubes during cooldown by steam at temperatures between 1100°C-1600°C have been performed.

- Large heat losses due to radiation prevent the onset of a temperature escalation.

- The β->α phase transition in the metal layer at about 850°C causes a deviation of the temperature from the regular cooldown curve.

- The post-test appearance of the oxidised Zr-1Nb tubes differs from that of Zircaloy-4. So, the Zr-1Nb oxide surface is considerably darker. Consequently the emissivity of oxidised Zr-1Nb tube surface can differ from the emissivity of oxidised Zircaloy-4 tube surface.

- Up to 1400°C the kinetics of the oxide layer growth on the Zr-1Nb surface is comparable with the kinetics of ZrO_2 layer growth on the Zircaloy-4 surface. Above 1400°C the oxidation rate is higher for Zr-1Nb.

- The micro cracks in the oxide layer on the Zr-1Nb tube distribute uniformly, whereas for Zircaloy-4 the micro cracks are preferably in the outer sub-layer of the oxide scale.

- The formation of macroscopic through-wall cracks can be observed by steam cooldown in experiments with ZrO_2 layer thickness larger than 200 µm (for Zircaloy-4 this boundary corresponds to 150 µm).

- In contrast to the Zircaloy-4 tests, the oxidation of crack surfaces was negligible.

- The amount of hydrogen production during the tests with Zr-1Nb rods was measured. Up to 1400°C this parameter is somewhat lower than for Zircaloy-4. It can be connected with a higher temperature heterogeneity along the tube axial direction in the Zr-1Nb test series than for Zircaloy-4 tests. Above 1400°C the rate of hydrogen production for Zr-1Nb steeply increases.

- The amount of absorbed hydrogen in segments of Zr-1Nb test specimens was analysed. The results show that the Zr-1Nb cladding tubes absorb less hydrogen than Zircaloy-4 under the same conditions.

- The SVECHA calculations show some overestimation of the oxide and alpha layer growth and correspondingly higher values for the hydrogen release. For that reason it is necessary to collect more experimental data, particularly for the temperature region between 1400°C and 1600°C.

5. References

1. P. Hofmann, V. Noack, M.S. Veshchunov, A.V. Berdyshev, A.V. Boldyrev, L.W. Matweev, A.V. Palagin, V.E. Shestak. Physico-chemical Behavior of Zircaloy Fuel Rod Cladding Tubes during LWR Severe Accident Reflood. FZKA 5846, May 1997

2. P. Hofmann, A. Miassoedov, L. Steinbock, M. Steinbrück, A.V. Berdyshev, A.V. Boldyrev, A.V. Palagin, V.E. Shestak, M.S. Veshchunov. Quench Behavior of Zircaloy Fuel Rod Cladding Tubes. Small-Scale Experiments and Modelling of the Quench Phenomena. FZKA 6208, March 1999

3. L. Steinbock, J. Stuckert. Determination of the Crack Pattern of Quenched Zircaloy Tubes. FZKA 6013, November 1997

4. S. Hagen, P. Hofmann, V. Noack, L. Sepold, G. Schanz. Comparison of the quench experiments CORA-12, CORA-13 and CORA-17. FZKA 5679, 1996

5. P. Hofmann, C. Homann, W. Leiling, A. Miassoedov, D. Piel, G. Schanz, L. Schmidt, L. Sepold, M. Steinbrück. Experimental and Calculational Results of the Experiments QUENCH-02 and QUENCH-03. FZKA 6295, July 2000

6. Private communication with Dr. Steinbock

7. A.V. Berdyshev, A.V. Boldyrev, A.V. Palagin, V.E. Shestak, M.S. Veshchunov, SVECHA/QUENCH Code for The Modeling of Reflooding Phenomena in Severe Accidents Conditions. Proceedings of the Ninth International Topical Meeting on Nuclear Reactor Thermal Hydraulics (NURETH-9), paper Log_19 (CD-ROM edition), San Francisco, California, 1999

Element	Zr-1Nb	Zircaloy-4
Nb	0.971 ± 0.004	-
Sn	< 0.004	1.525 ± 0.011
Hf	0.0252 ± 0.0001	< 0.005
Fe	0.0079 ± 0.0002	0.221 ± 0.001
Cr	0.0022 ± 0.00005	0.105 ± 0.001
Ni	0.0023 ± 0.0001	-
Ca	< 0.005	< 0.005
Y	< 0.003	< 0.002
Cu	< 0.0003	-
Mn	0.00007 ± 0.00001	-
O	0.046 ± 0.002	0.135 ± 0.015
N	0.004 ± 0.001	0.007 ± 0.005

Table 1. Chemical analysis results of Zr-1Nb and Zircaloy-4 cladding materials

Test No.	Test name	Mass gain, protect., mg	Calc.* ZrO_2 thick., µm	Oxidation at 1400°C, minutes	Quench temp., °C (pyr.)	Eff. oxide layer# (eddy-current), µm			Mass gain, mg	Radius increase max, µm	Calculated** Oxide thick., max, µm	Length increase, mm
						low	mid	up				
9	28030b	78	9	19	1100°C	276	482	225	1609	85 ± 5	**255** ± 15	0.70
7	27030b	70	8	7	1200°C	181	220	146	0944	50 ± 5	**150** ± 15	0.85
3	20030b	71	8	12	1200°C	297	352	221	1404	60 ± 5	**180** ± 15	
6	27030a	64	7	19	1200°C	189	443	212	1543	75 ± 5	**225** ± 15	1.54
2	20030a	70	8	25	1200°C	390	714	279	1924	105 ± 5	**315** ± 15	
5	24030	75	9	13.5	1400°C	238	345	198	1288	55 ± 5	**165** ± 15	0.85
1	17030	91	11	18.5	1400°C	230	423	201	1621	80 ± 5	**240** ± 15	1.00
8	28030a	71	8	26.5	1400°C	268	664	239	1561	95 ± 5	**285** ± 15	0.70
4	21030	124	15	6	1600°C	246	536	228	2072	145 ± 5	**435** ± 15	1.20

eddy device calibration was carried out on the sample without α-Zr(O) layer, for that reason the real ZrO_2 layer is thinner

* protection oxide layer average thickness $\delta_p = m_{ZrO2}/d_{ZrO2}/(\pi \bullet L \bullet D)$, where tube diameter D=9.13 mm, tube length L=150 mm, density d_{ZrO2}=5.68 g/cm³, mass $m_{ZrO2}=(\Delta_m-\Delta_m/4)\bullet\mu_{ZrO2}/\mu_{O2}$, Δ_m – oxygen mass (probe mass gain), $\Delta_m/4$ ~ oxygen mass in the α-Zr(O) layer, μ_{ZrO2}=123.2 g/mol, μ_{O2}=32 g/mol

** oxide layer thickness $\delta=\Delta_R \bullet 2 \bullet B$, where Δ_R – radius increase of the tube middle part, Pilling-Bedworth ratio B=1.5

Table 2: Test matrix and post-test non-destructive measurement results

Test number	Test date	Oxidation at 1400°C minutes	Quench temp. °C (pyrom.)*	Macroscopic post-test appearance	Oxide layer (metallography), µm			α-Zr(O) layer (metallography), µm			β-Zr layer (metallography), µm			Presence of penetrating cracks		
					low**	mid	up	low	mid	up	low	mid	up	low	mid	up
9	28030b	19	1100°C	brittle	215	285	114	319	503	161	225	0	425		Yes	
7	27030b	7	1200°C	stable	113	152	95	115	134	64	526	464	570	No	No	No
3	20030b	12	1200°C	brittle	167	184	110	185	275	157	387	275	450		No	
6	27030a	19	1200°C#	brittle	138	202	109	205	267	140	358	271	448		Yes	
2	20030a	25	1200°C	brittle	199	370	165	236	437	206	294	0	355	No	Yes	
5	24030	13,5	1400°C#	stable	165	202	117	273	282	168	323	291	495	No	Yes	No
1	17030	18,5	1400°C	brittle	195	285	155	303	516	275	271	0	328	Yes	Yes	No
8	28030a	26,5	1400°C#	brittle	175	281	154	242	489	190	301	0	388		Yes	
4	21030	6	1600°C#	stable	199	547	133	186	324	139	387	0	486	No	Yes	No

* - Pyrometer measurements correspond to central TC; lower and upper TC are cooler by ~70K and ~150K
# - lower TC failed
** - low - elevation 30 mm, mid - elevation 75 mm, up - elevation 120 mm

Table 3: Mechanical properties and layer thicknesses

Test Number	Oxidation at 1400°C minutes	Quench temp. °C (pyrom.)	Oxide layer, elev. 75 mm, 120 mm µm	**H_2 production** maximum mg/s	integr. mg	quench / integr.	Corresponding Zircaloy-4 experiments Oxide layer µm	**H_2 production** mg
9	19	1100	285, 114	0.279	**220.3**	**0.026**	270 (mid), 255 (up)	**244.5**
7	7	1200	152, 95	0.265	**121**	**0.062**	167	**184.8**
3	12	1200	184, 110	0.283	**183**	**0.043**	212 (mid), 210 (up)	**239.5**
6	19	1200	202, 109	0.267	**204**	**0.025**		
2	25	1200	370, 165	0.286	**268**	**0.038**	310	**295**
5	13.5	1400	202, 117	-	**-**		-	**203.7**
1	18.5	1400	285, 155	0.271	**222.8**	**0.076**	263	**244**
8	26.5	1400	281, 154	0.258	**251.5**	**0.062**	335	**330**
4	6	1600	547*, 133	0.294	**376.5**	**0.374**	370	**170.2**

* TC value to the QUENCH time was 1700°C

Table 4: Hydrogen production during the pre-oxidation and steam cooldown. Comparison with corresponding Zircaloy-4 experiments

Test date	Oxidation at 1400°C minutes	Quench temp. °C (pyrom.)	Oxide layer* µm	**H_{abs} concentr.*** ref. to metal mole %			Ratio** H_{abs}/H_{prod}	Corresponding Zircaloy-4 specimens	
				low	middle	up		Oxide layer* µm	**H concentration* mole %**
28030b	19	1100°C	285	**0.47**	**0.47**	**0.52**	**0.011**	270, 255	**1.47**
27030b	7	1200°C	152	**0.24**	**0.27**	**0.52**	**0.016**	167	**0.22**
20030b	12	1200°C	184	**0.70**	**0.24**	**1.09**	**0.015**	212	**1.43**
27030a	19	1200°C	202	**0.53**	**0.67**	**0.44**	**0.014**	*** 220/240	*** **1.0/3.98**
20030a	25	1200°C	370	**0.80**	**1.43**	**0.52**	**0.012**	-	
24030	13.5	1400°C	202	**0.56**	**0.66**	**0.97**		-	
17030	18.5	1400°C	285	**0.42**	**1.16**	**0.62**	**0.016**	263	**2.05**
28030a	26.5	1400°C	281	**0.53**	**1.02**	**0.47**	**0.013**	-	
21030	6	1600°C	547	**2.35**	**0.68**	**0.58**	**0.016**	370	**3.02**

* 10 mm probes taken from the lower, middle and upper part of the each tube section (three sections: 0-50 mm, 50-100 mm, 100-150 mm)

**H_{abs} - average value for specimens from the lower part, middle part and upper part of the tube

*** - series 1997 with other cooldown conditions: 1.0 mol% corresponds to 0.08 g/s steam rate on the cooldown, 3.98 mol% corresponds to 1.5 g/s of steam rate on the cooldown

Table 5: Results of the analysis of the hydrogen absorbed in the specimens. Comparison with corresponding Zircaloy-4 experiments

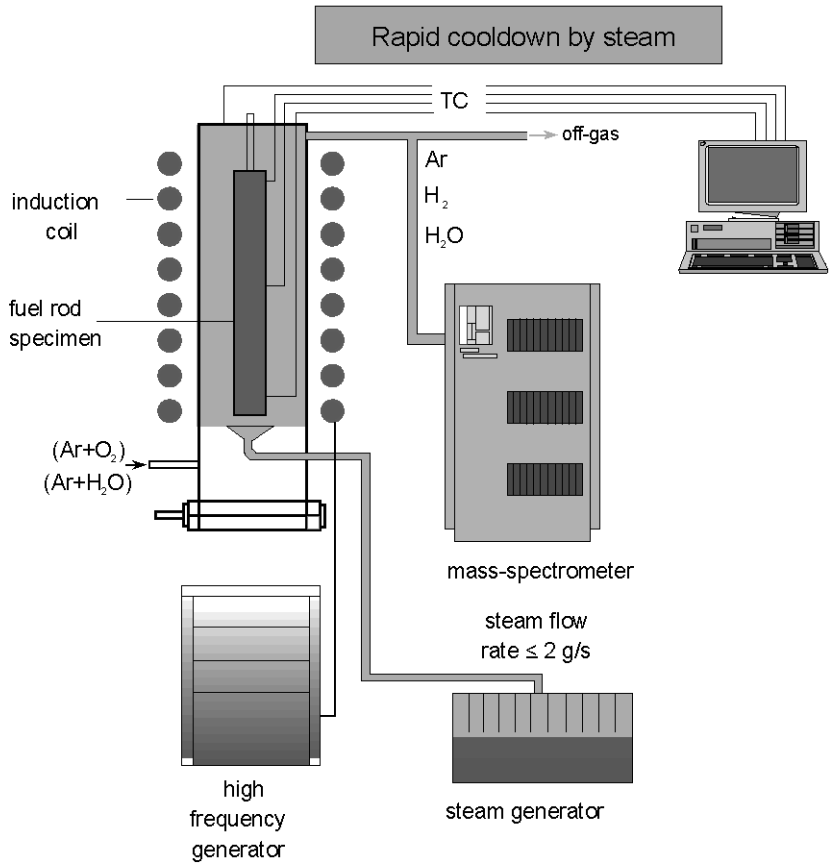

Fig. 1: Quench apparatus simulating steam cooldown conditions of an overheated fuel rod

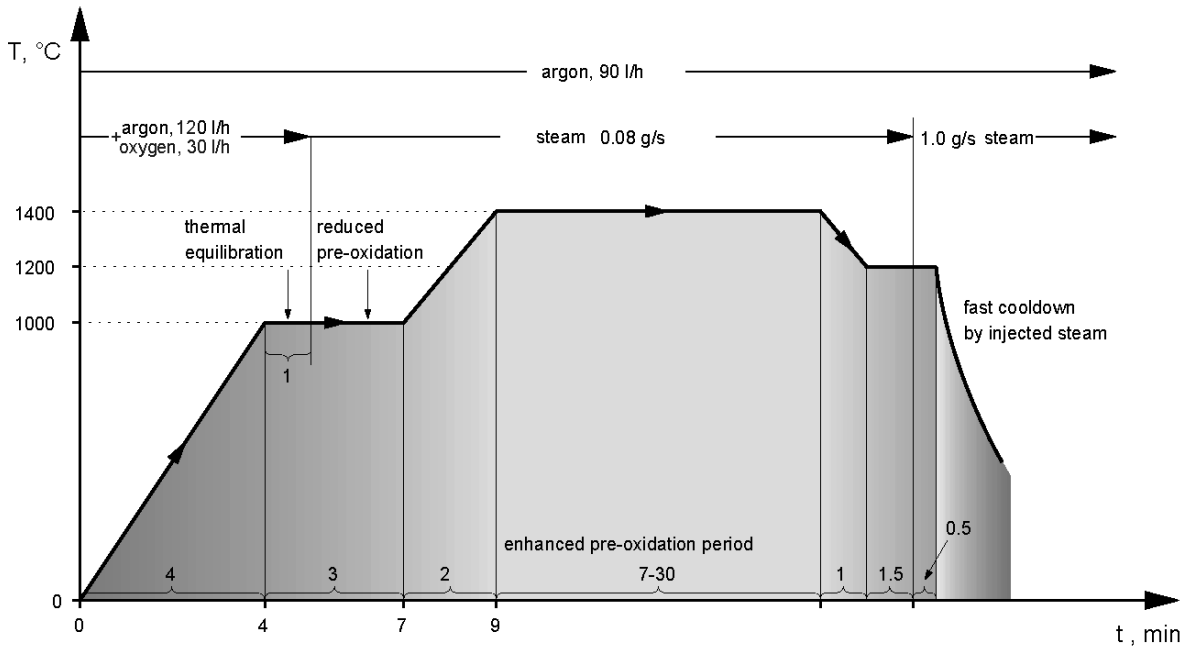

Fig. 2: Test conduct of single rod quench experiments

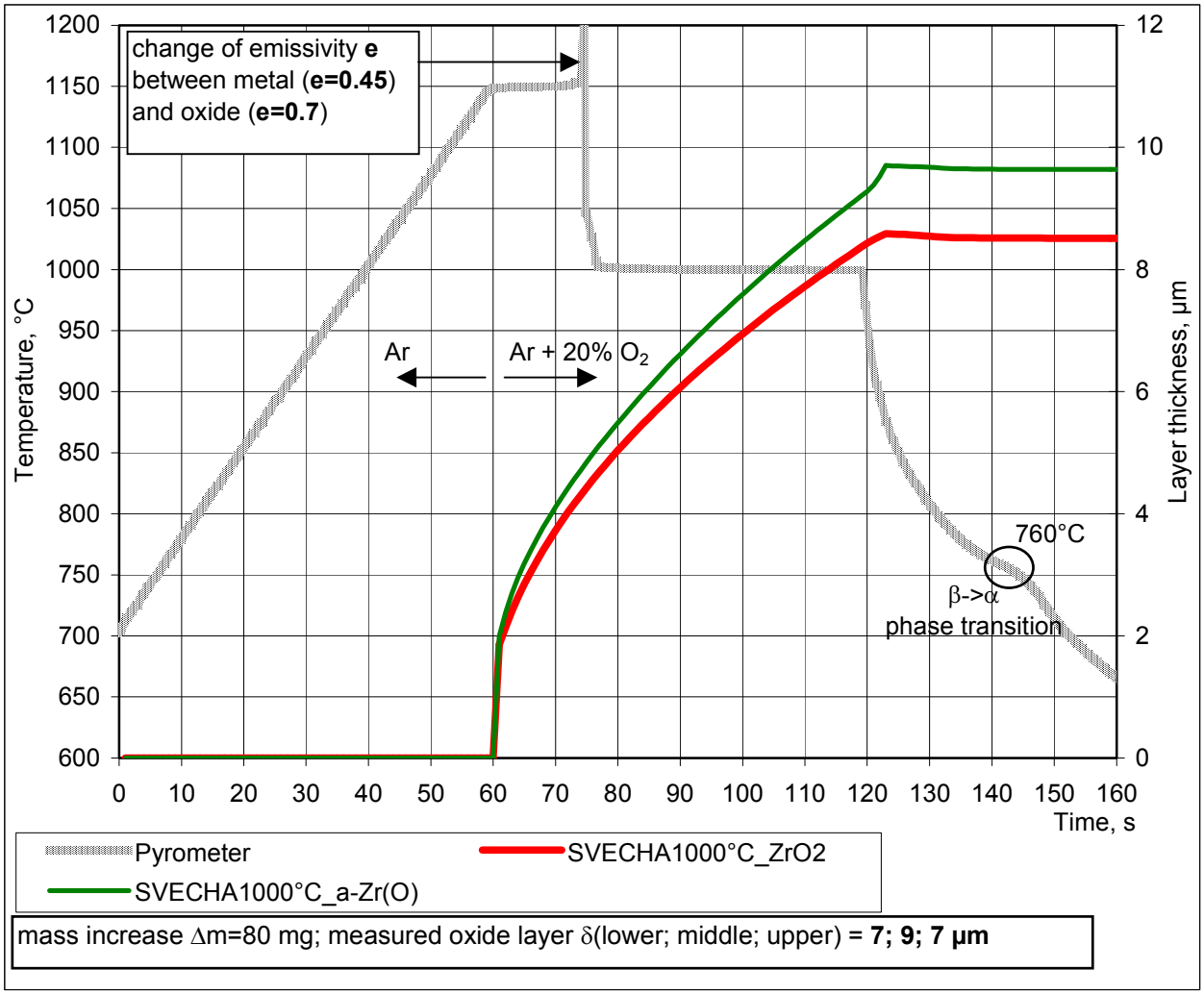

Fig. 3: Pre-oxidation at 1000°C for the formation of an insulating oxide layer to prevent eutectic interaction between TC and cladding; Ar 120 l/h+O_2 30 l/h. Experimental and calculation results

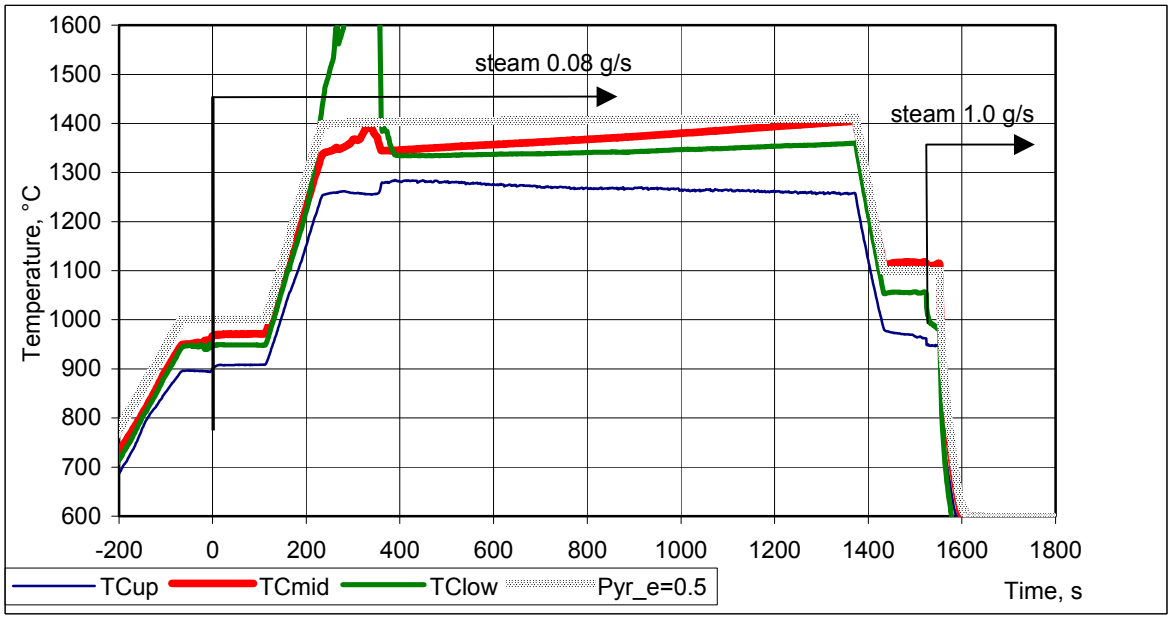

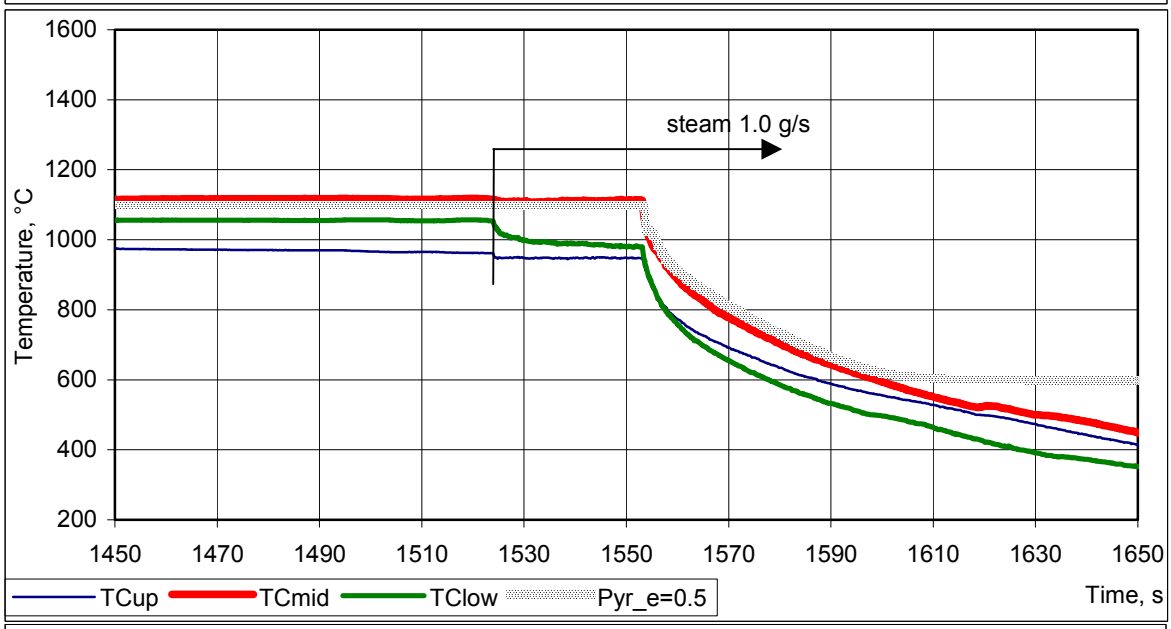

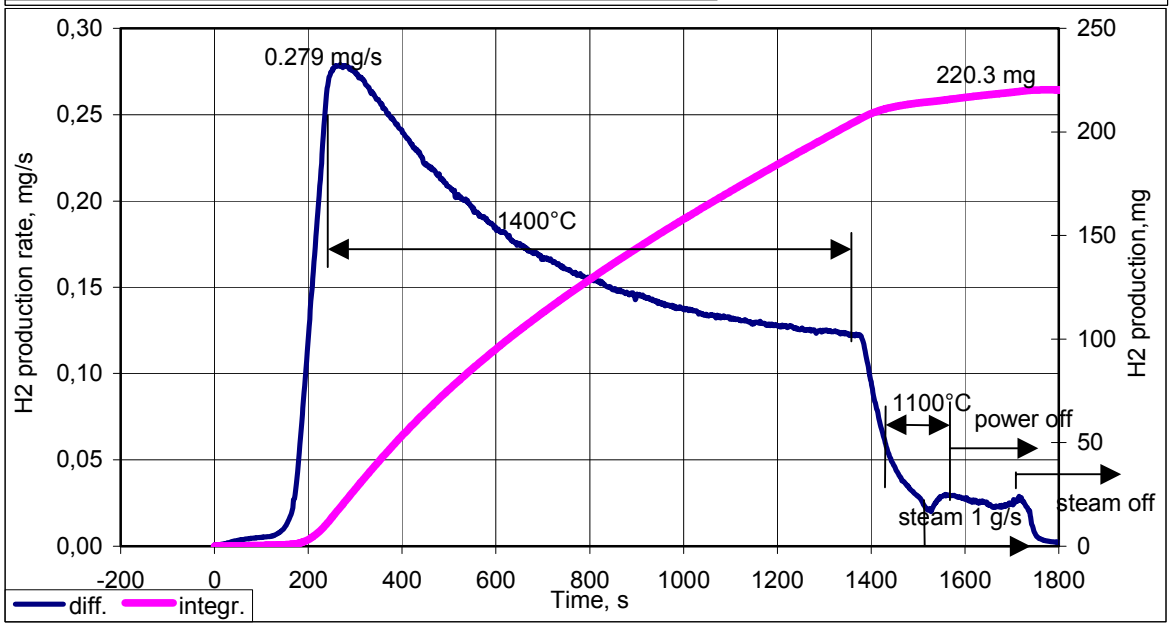

Fig. 4: Temperature history and corresponding hydrogen release for the test No. 9 (28030b). Pre-oxidation 19 minutes, cooldown from 1100°C

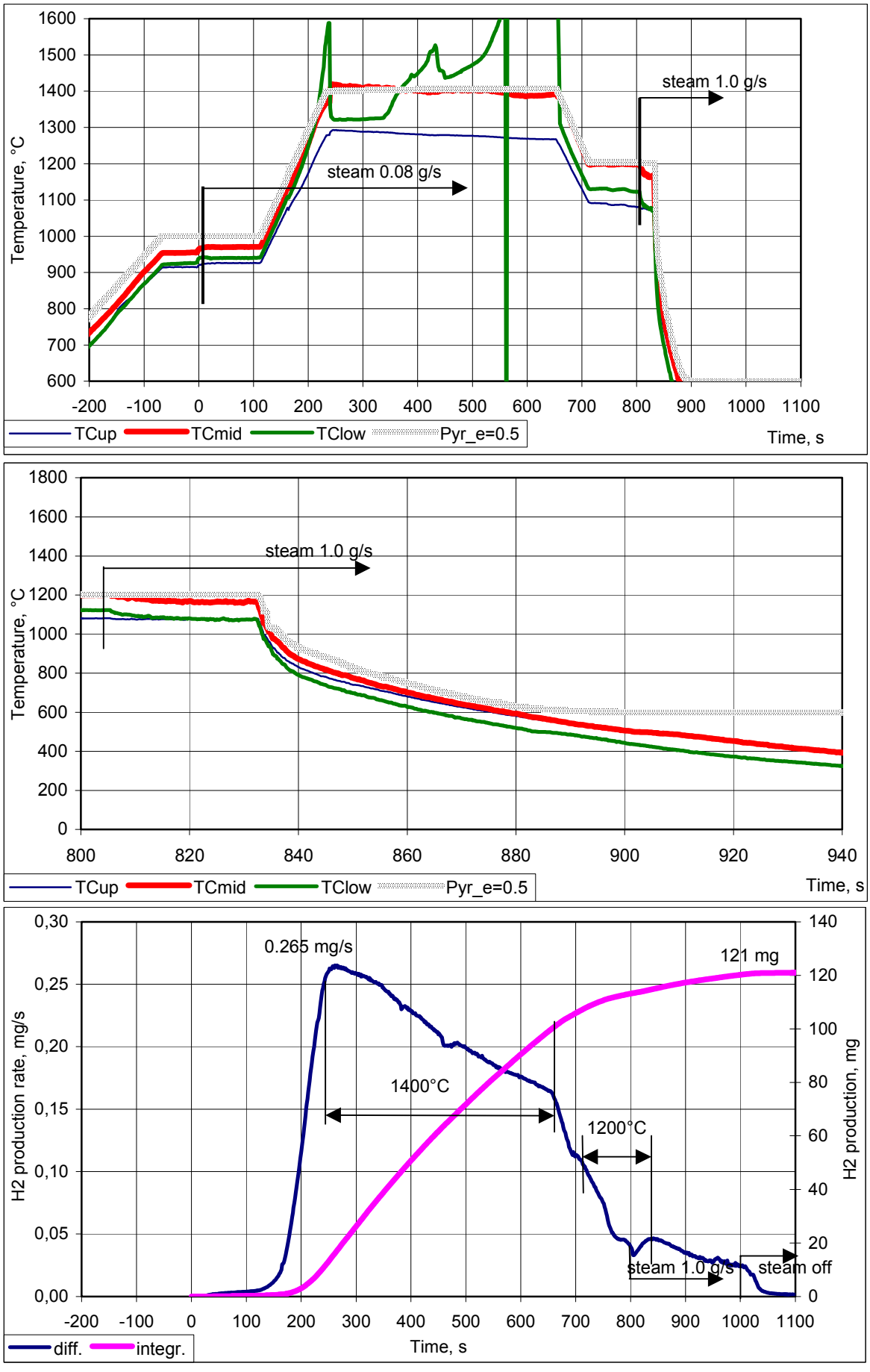

Fig. 5: Temperature history and corresponding hydrogen release for the test No. 7 (27030b). Pre-oxidation 7 minutes, cooldown from 1200°C

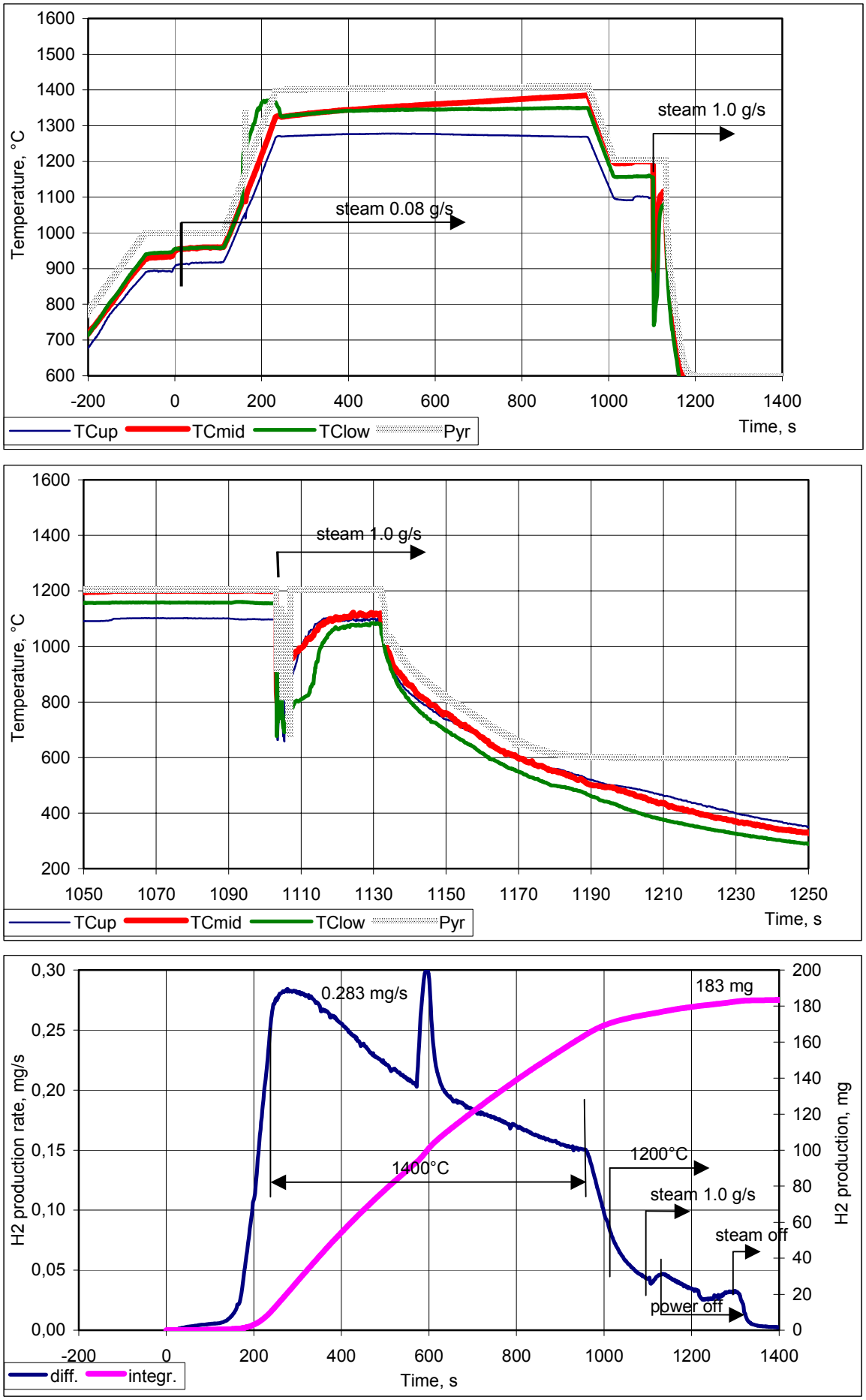

Fig. 6: Temperature history and corresponding hydrogen release for the test No. 3 (20030b). Pre-oxidation 12 minutes, cooldown from 1200°C

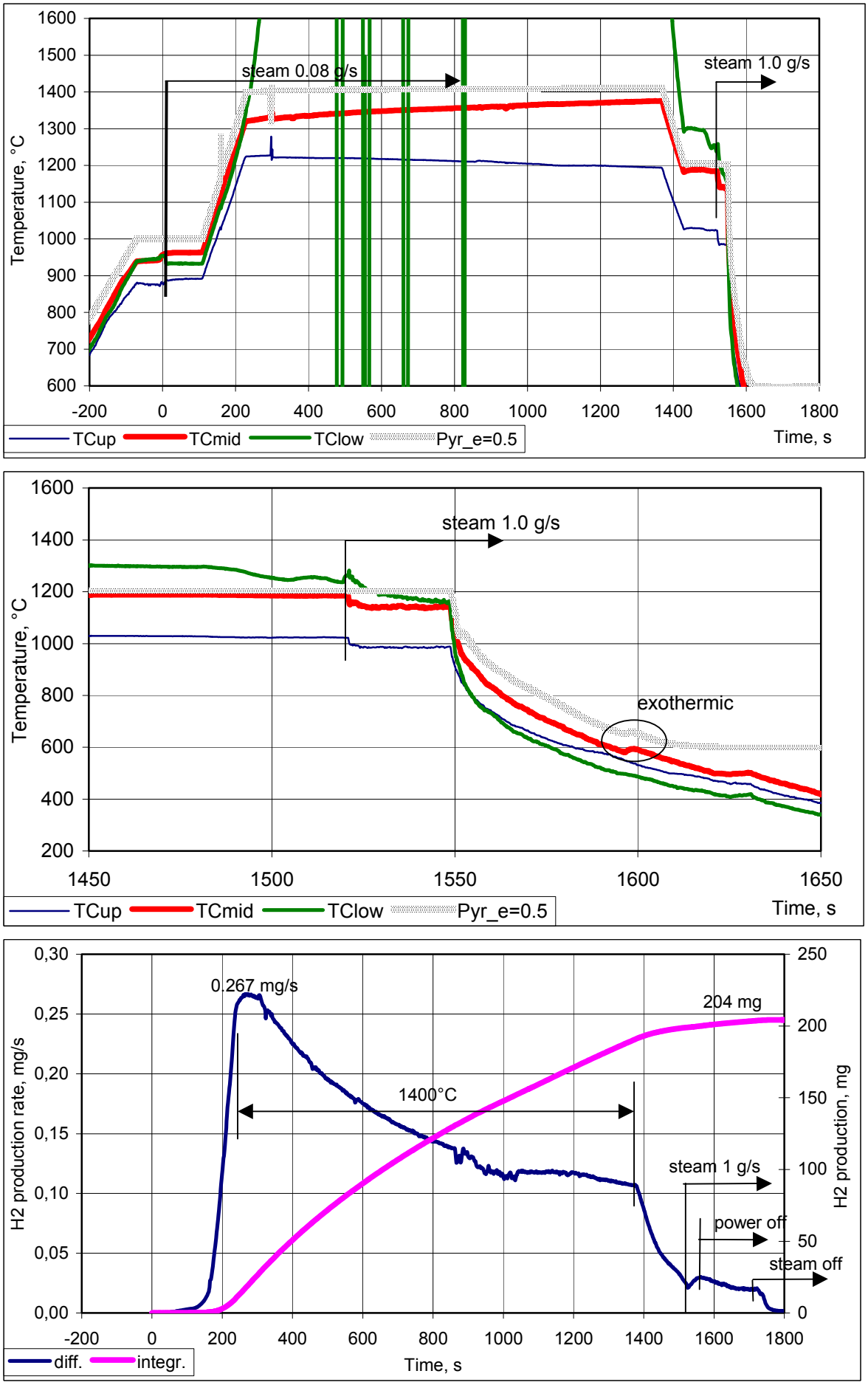

Fig. 7: Temperature history and corresponding hydrogen release for the test No. 6 (27030a). Pre-oxidation 19 minutes, cooldown from 1200°C

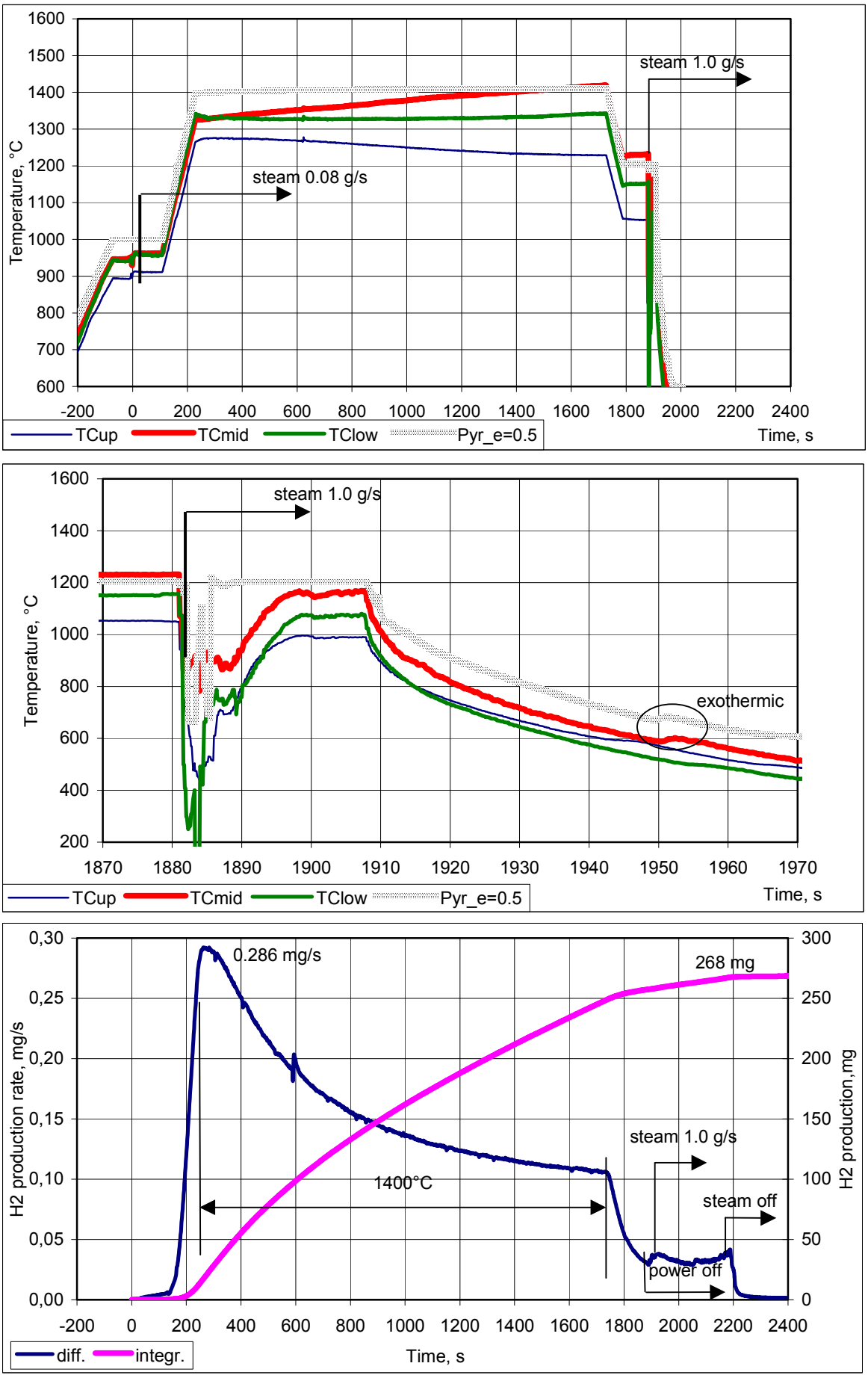

Fig. 8: Temperature history and corresponding hydrogen release for the test No. 2 (20030a). Pre-oxidation 25 minutes, cooldown from 1200°C

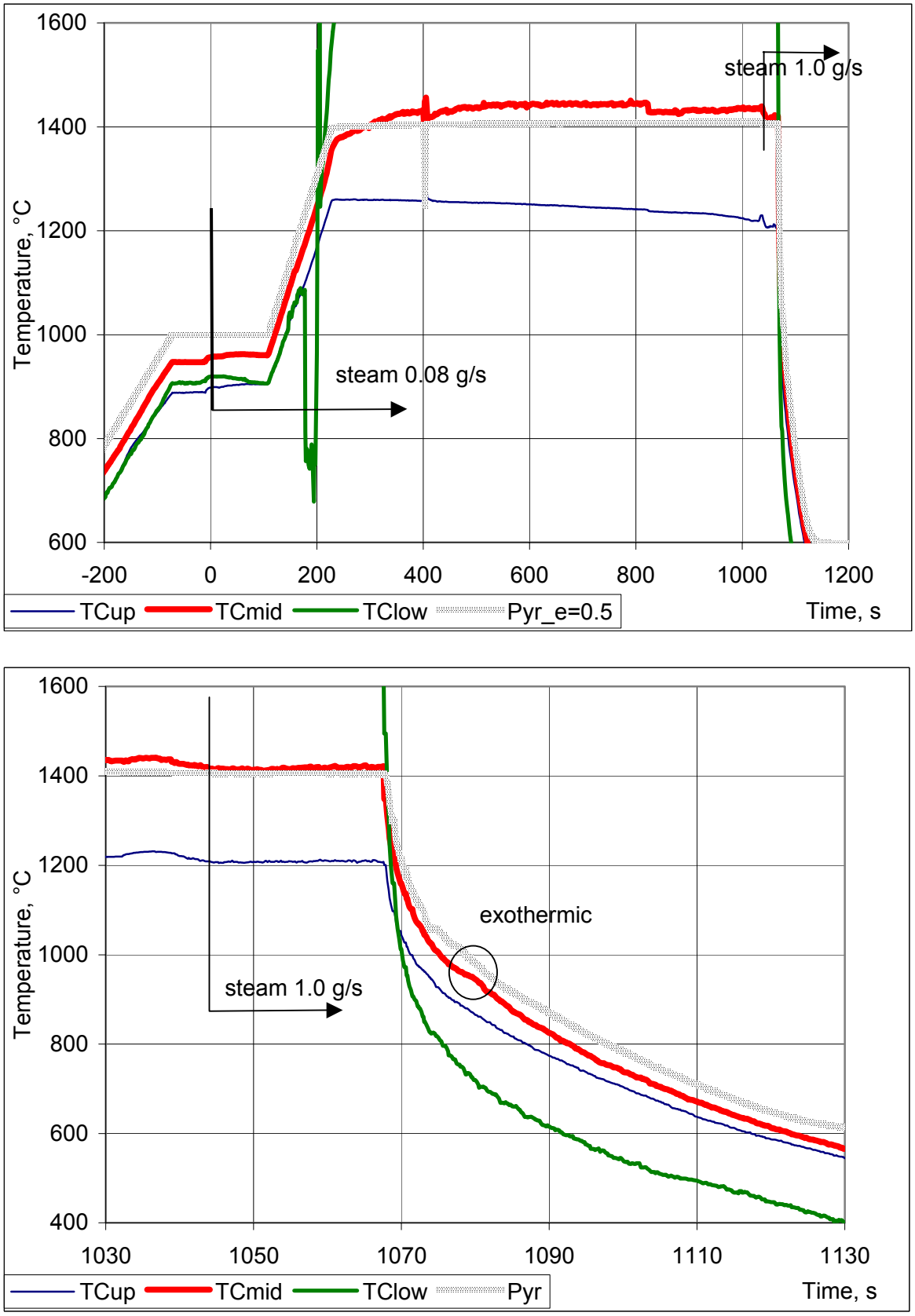

Fig. 9: Temperature history for the test No. 5 (24030). Pre-oxidation 13.5 minutes, cooldown from 1400°C

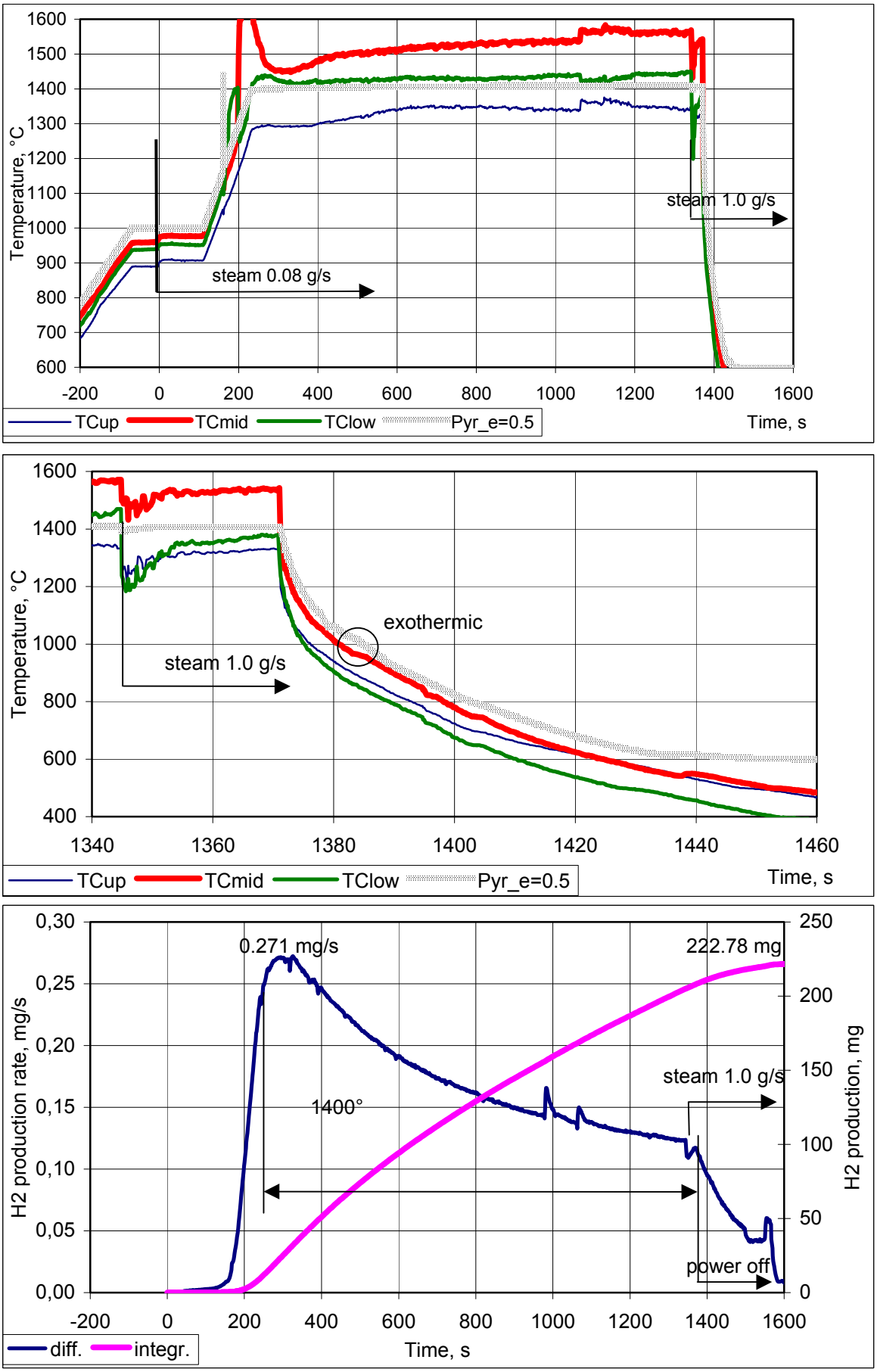

Fig. 10: Temperature history and corresponding hydrogen release for the test No. 1 (17030). Pre-oxidation 18.5 minutes, cooldown from 1400°C

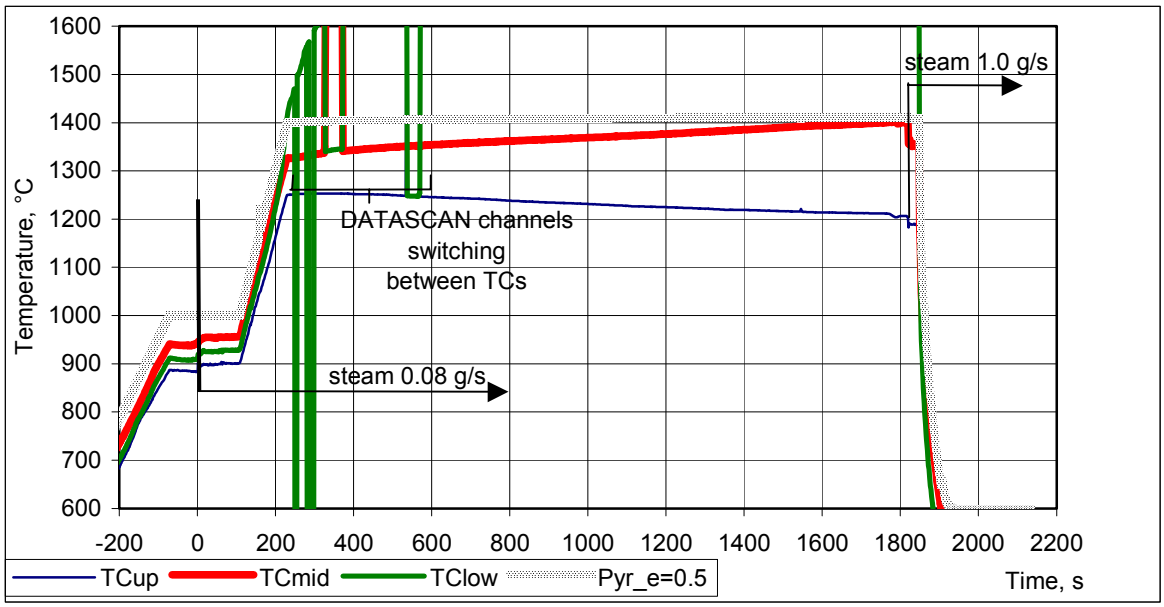

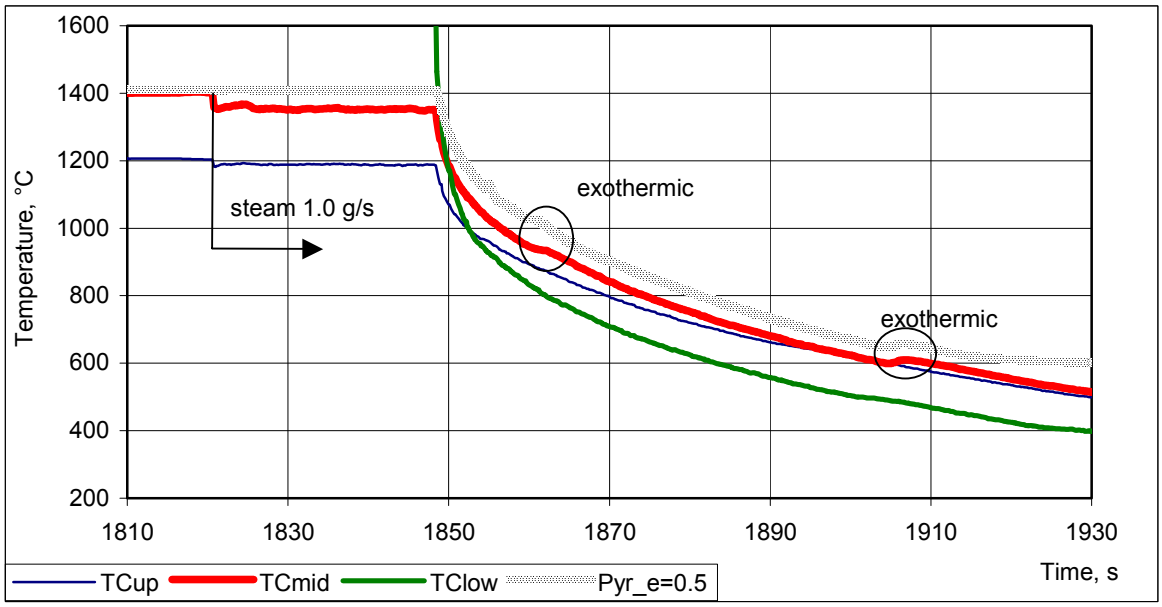

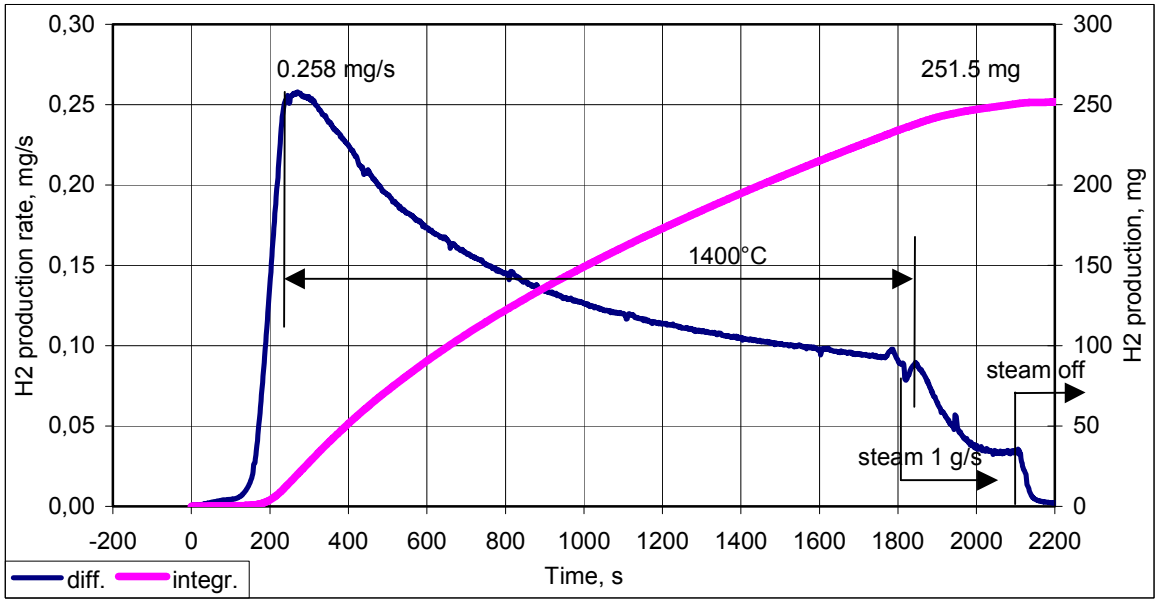

Fig. 11: Temperature history and corresponding hydrogen release for the test No. 8 (28030a). Pre-oxidation 26.5 minutes, cooldown from 1400°C

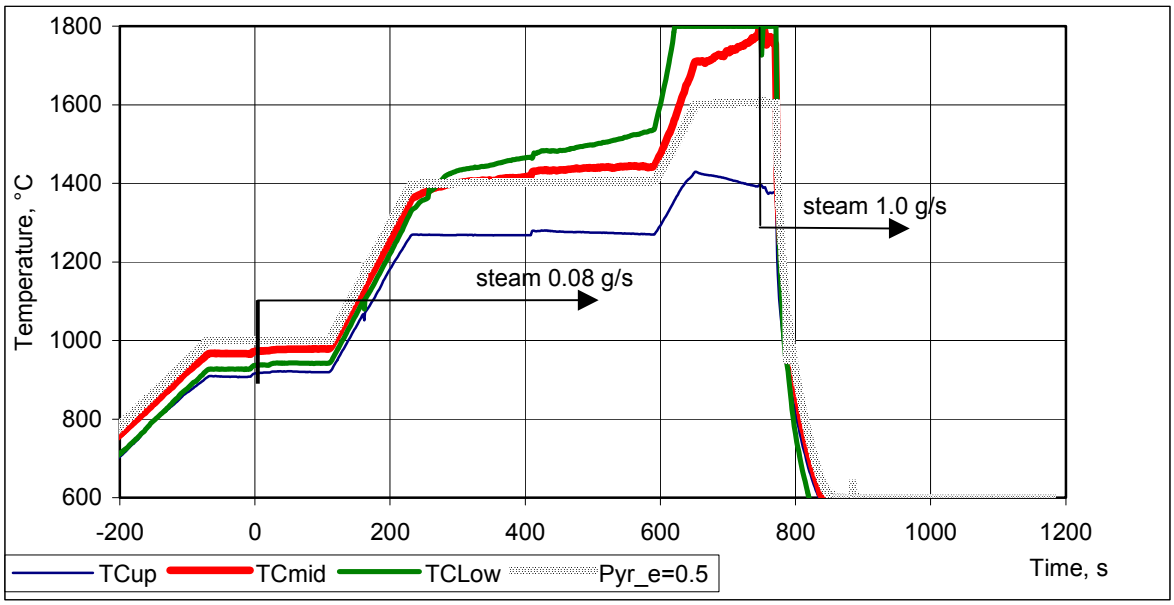

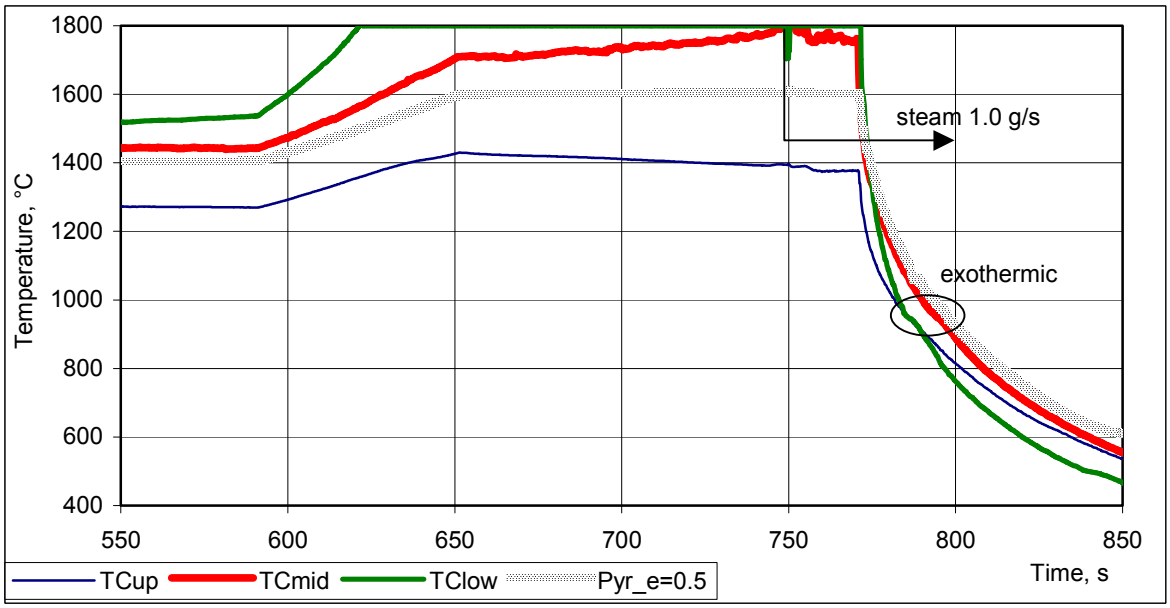

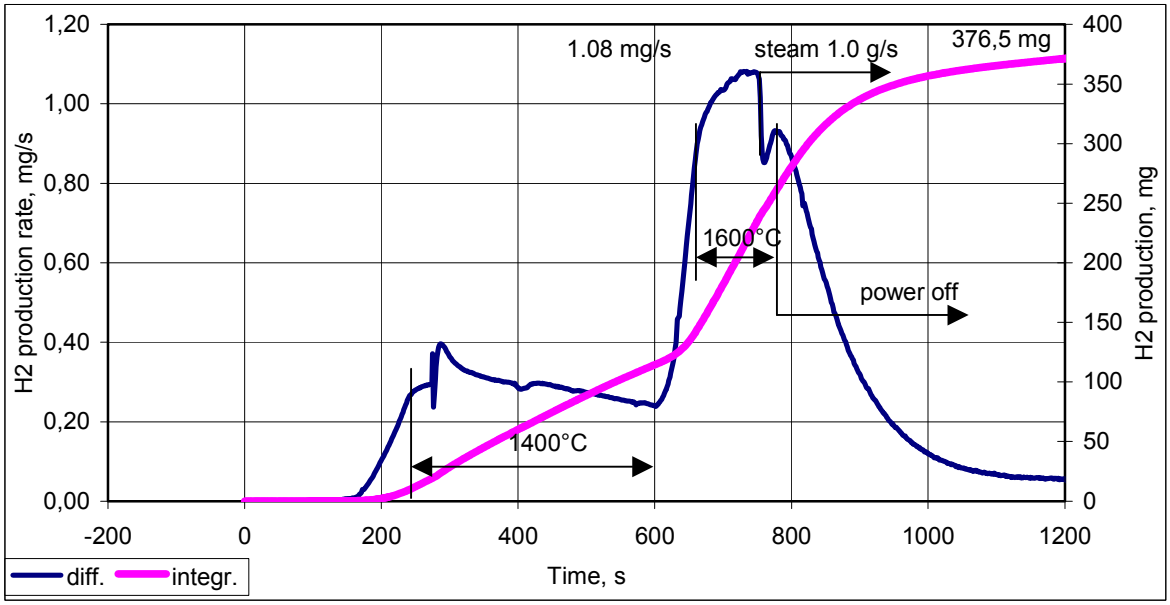

Fig. 12: Temperature history and corresponding hydrogen release for the test No. 4 (21030). Pre-oxidation 6 minutes, cooldown from 1600°C

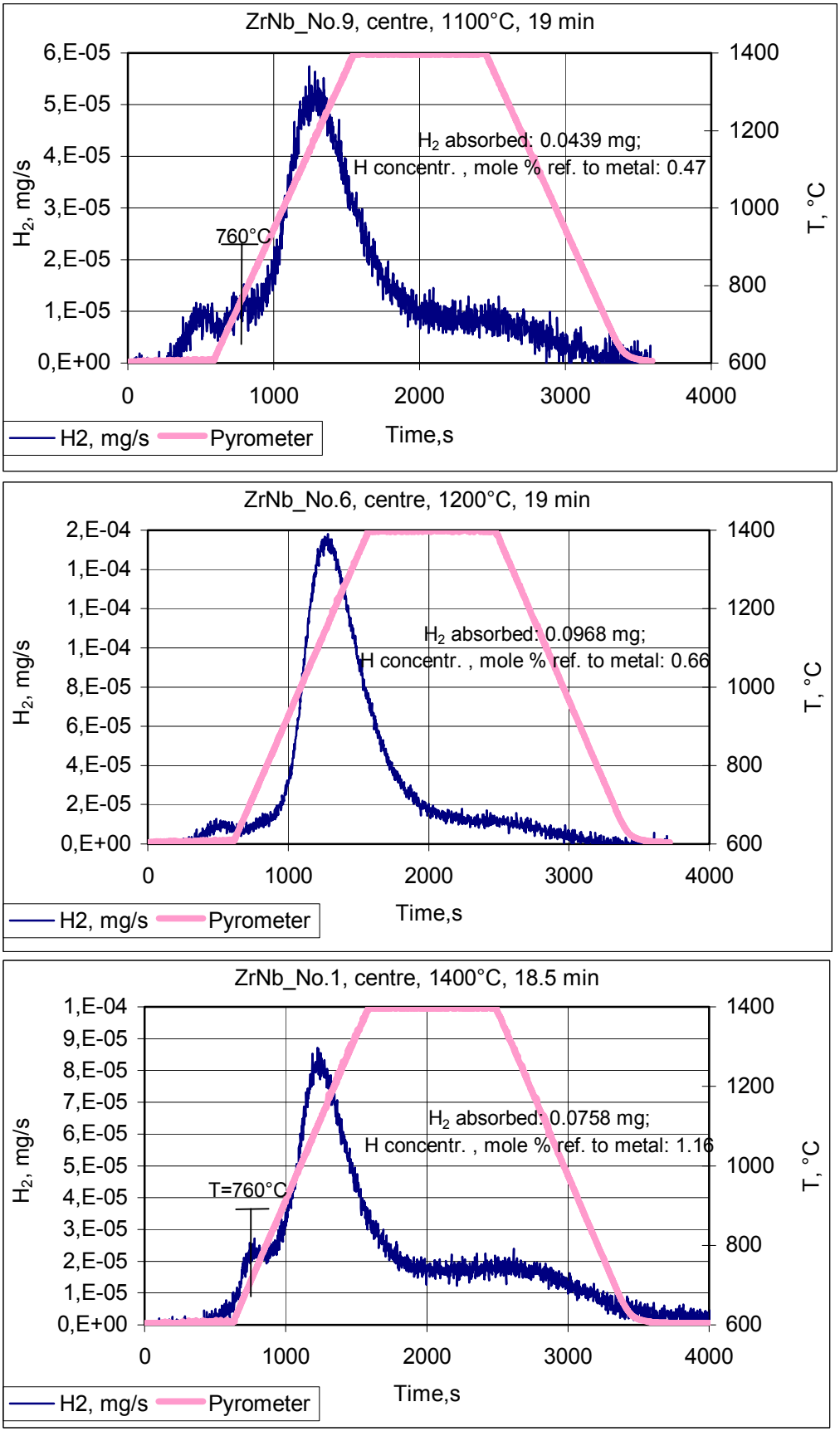

Fig. 13: Analysis of hydrogen absorbed in cladding tube segments at elevation 65-75 mm. Typical curve profiles from LAVA rig

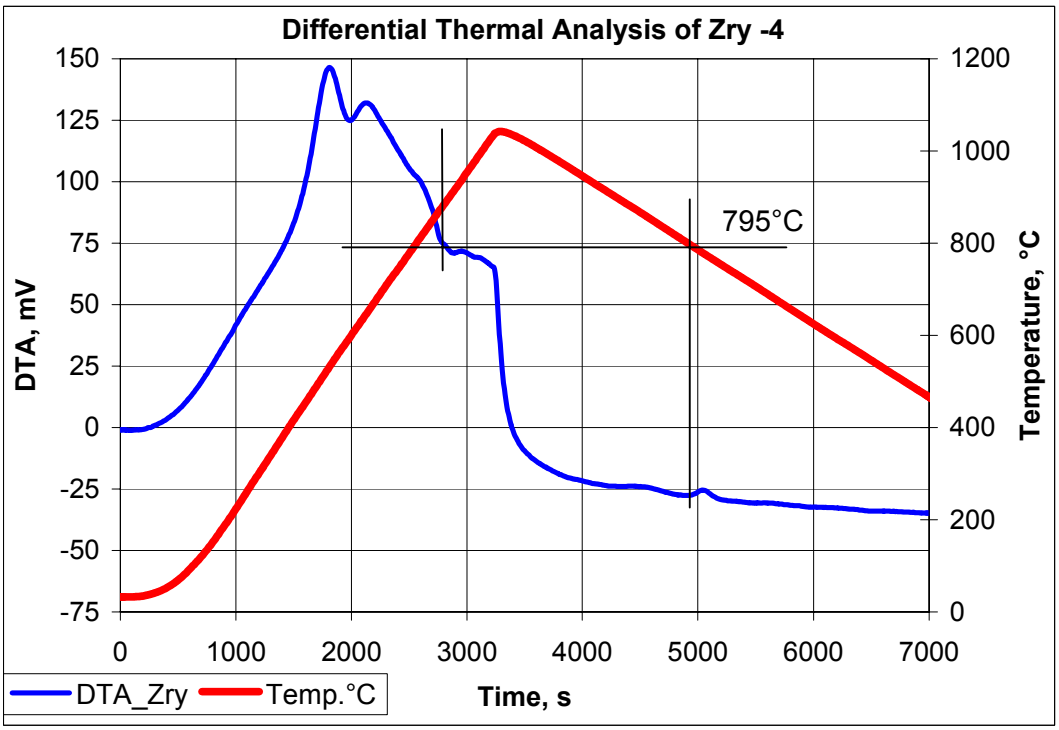

(a)

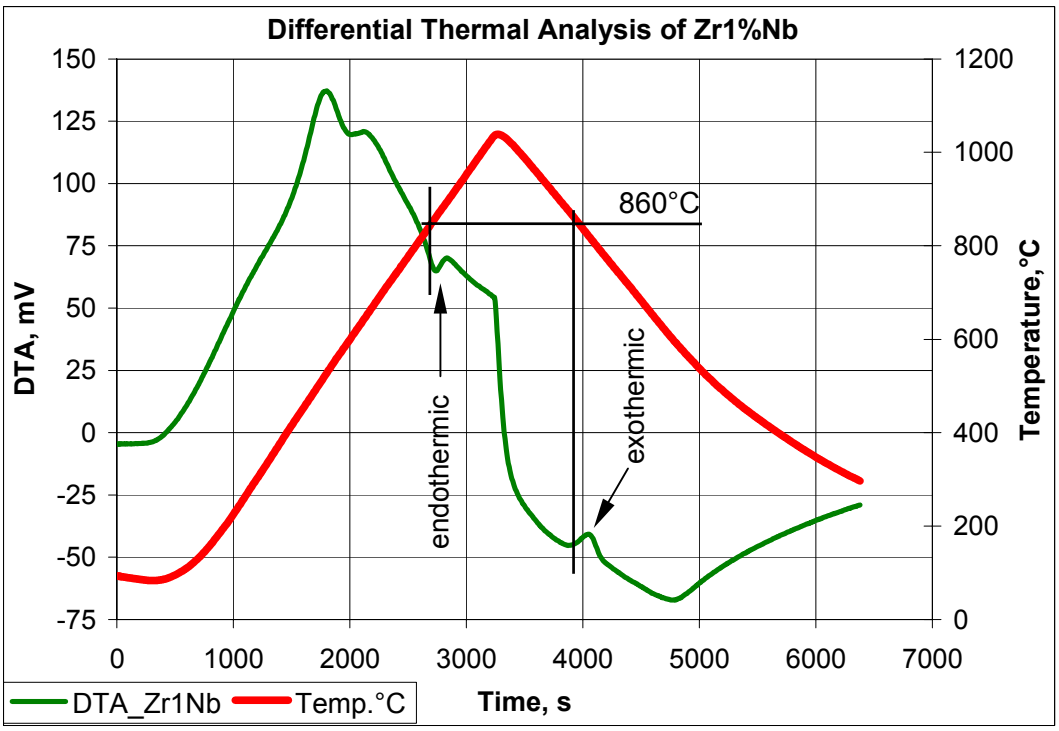

(b)

Fig. 14: : Differential thermal analysis performed for two kinds of materials: a) Zircaloy-4; and b)Zr-1Nb. Probe dimensions: disc diameter 9.1 mm, thickness 2 mm

Fig. 15: Macroscopic appearance of stable specimens

Fig. 16: Macroscopic appearance of brittle specimens

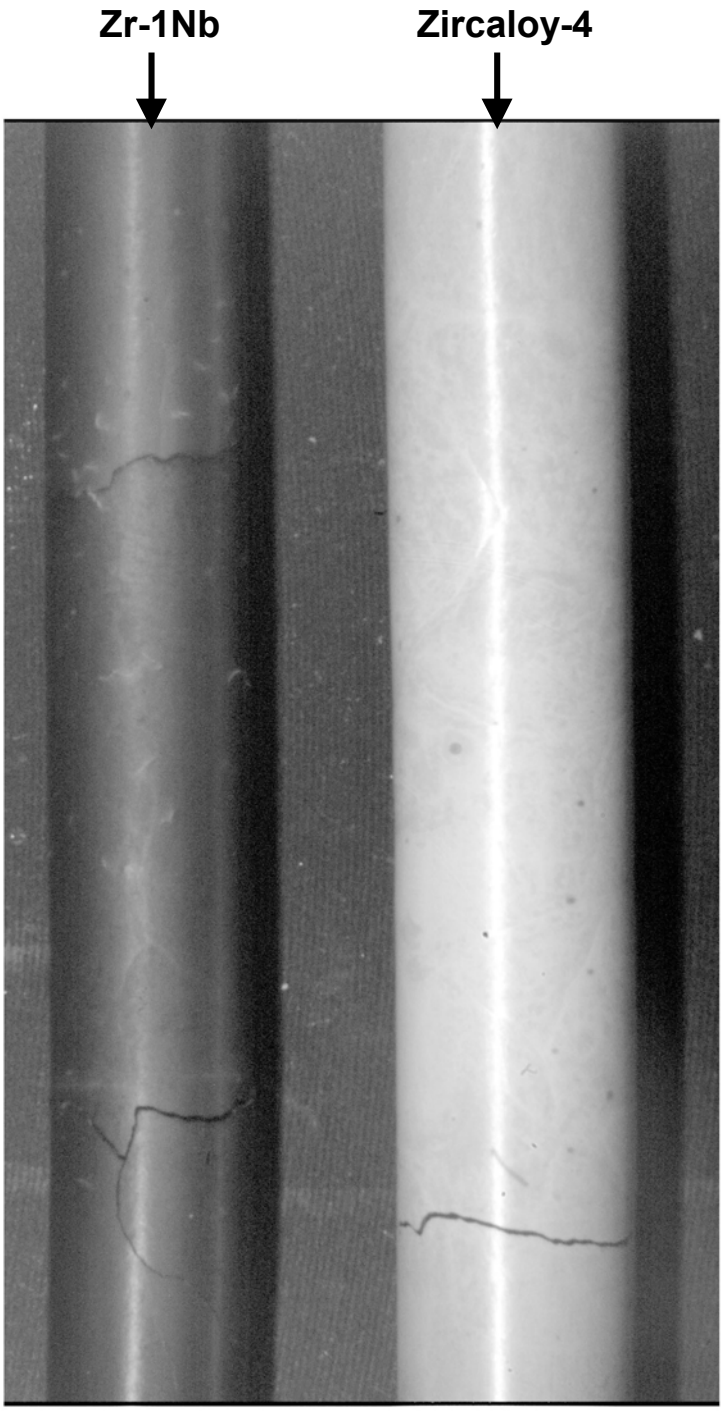

Fig. 17: Comparison between two cladding types after cooldown by steam at 1400°C. Duration of pre-oxidation 19 min

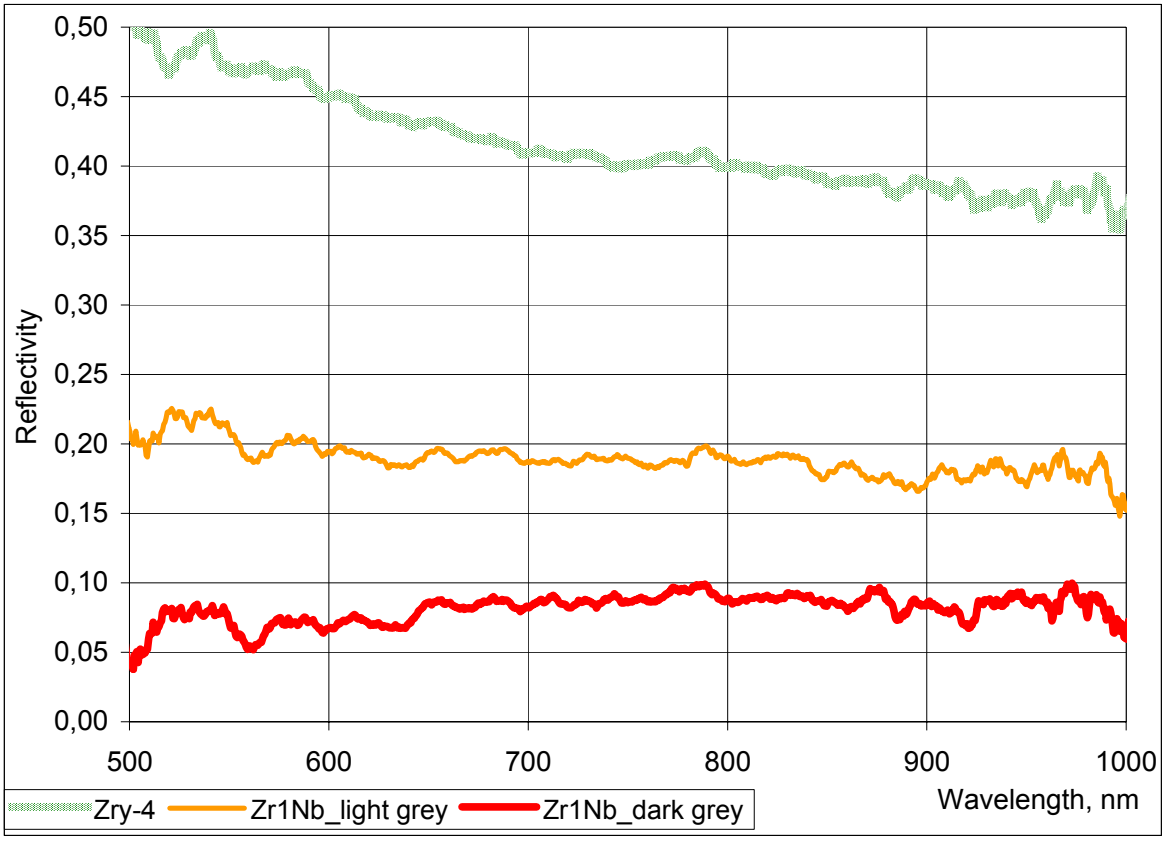

Fig. 18: Reflectivity of oxidised cladding at 20°C, oxide layer thickness ~250µm

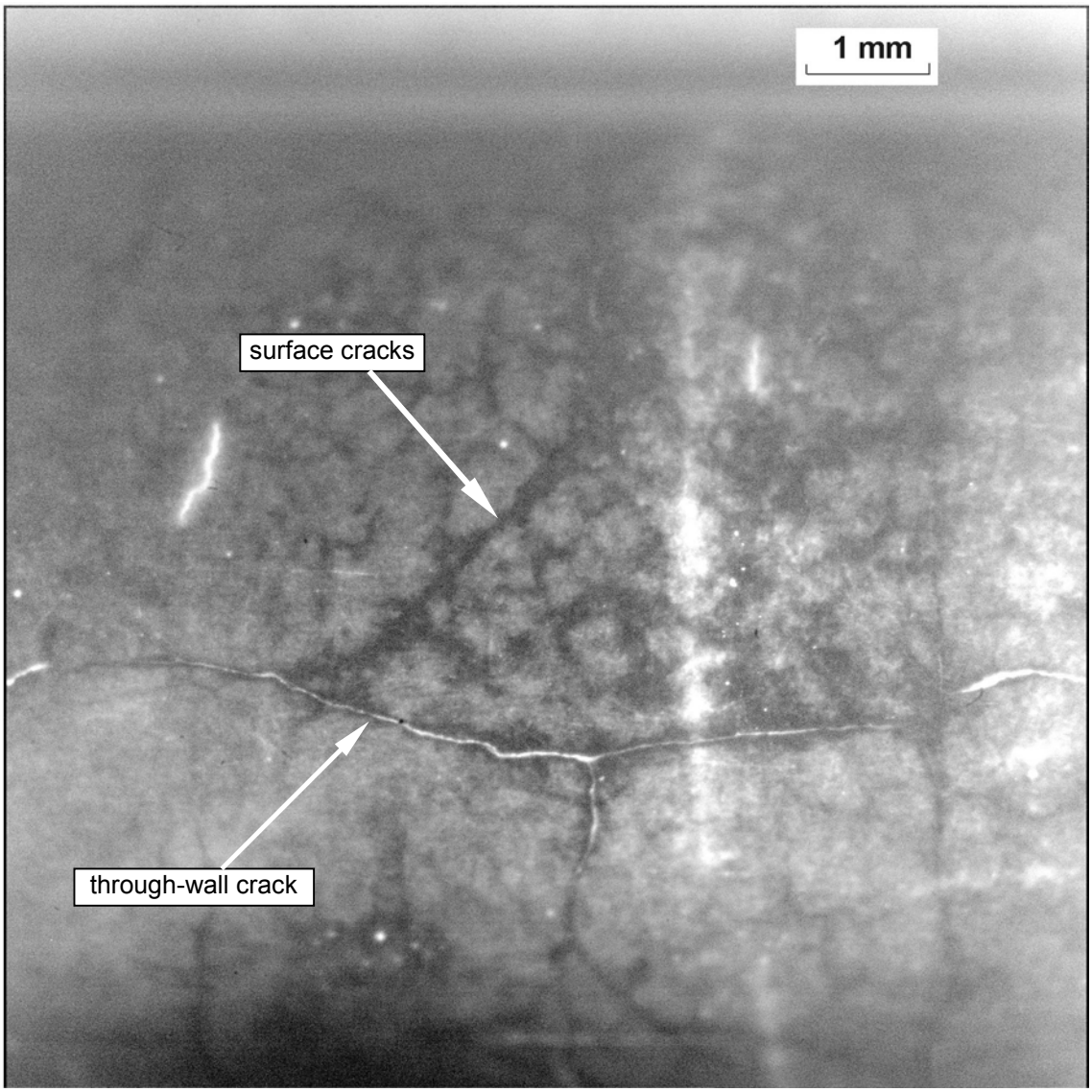

Fig. 19: Crack formation on the surface of the cladding tube. Specimen No. 1 after solvent injection. Steam cooldown from 1400°C, oxide layer thickness 280 µm

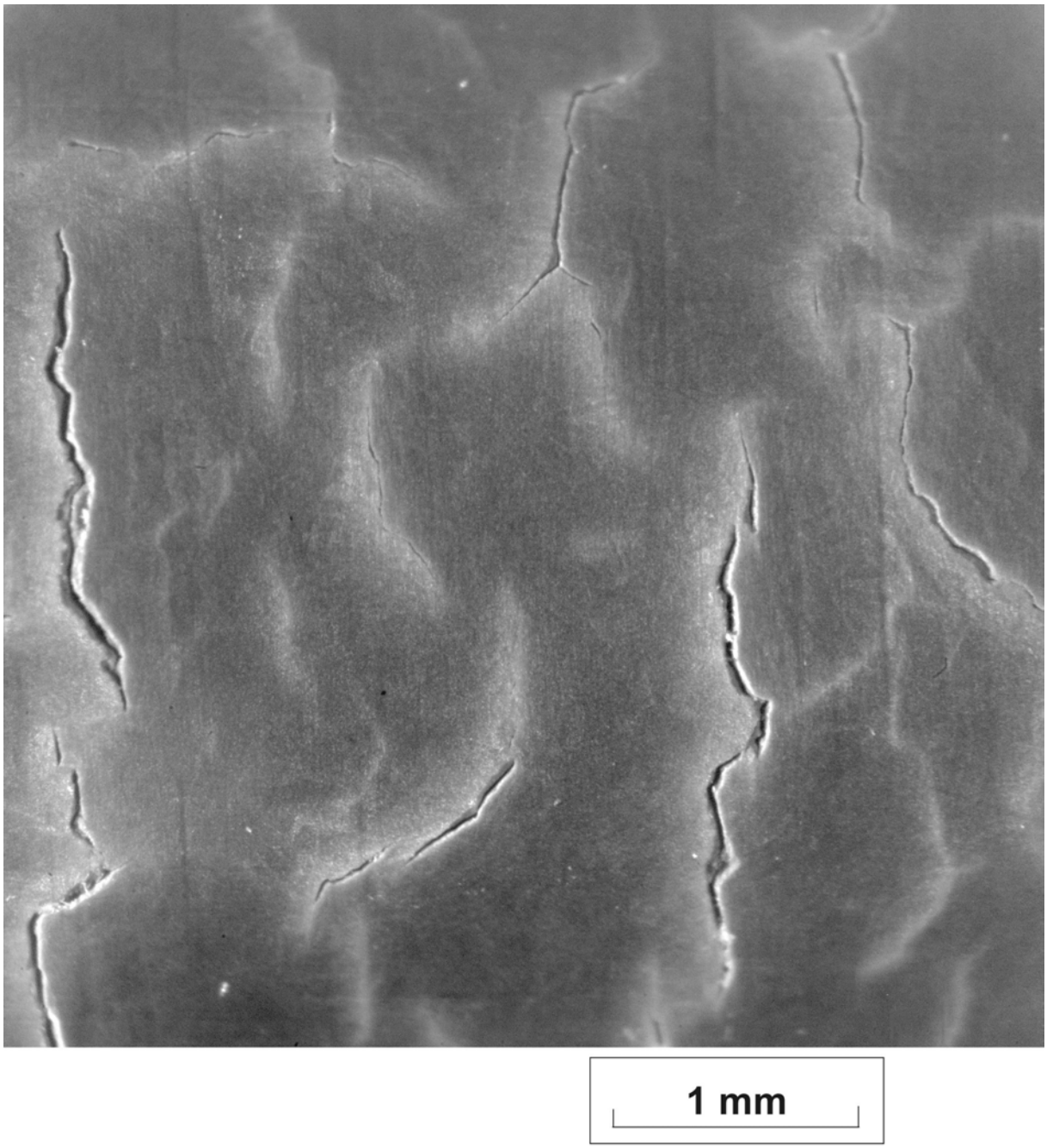

Fig. 20: Surface of the specimen No. 4. Steam cooldown from 1600°C, oxide layer ~500 µm. Cracks in the oxide layer

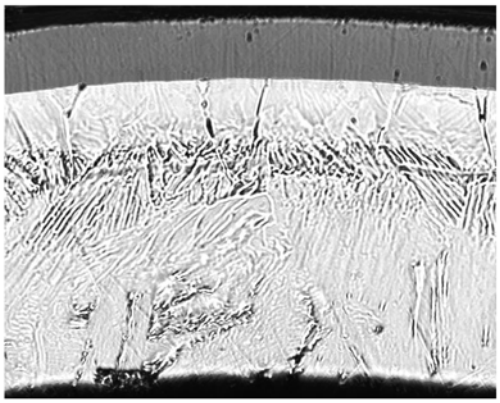

Elevation 120 mm
Max pre-oxidation temperature 1280°C

Elevation 75 mm
Max pre-oxidation temperature 1395°C

Elevation 30 mm
Max pre-oxidation temperature 1335°C

Fig. 21: Test No. 9 (pre-oxidation period 19 min., cooldown from 1100°C). Cross sections at three TC elevations, as polished.
There are a few non-oxidised through-wall cracks

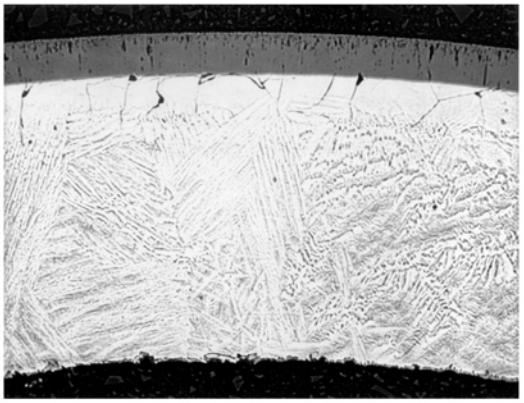

ZrO_2 95 µm
α-Zr(O) 64 µm
β-Zr 570 µm

Elevation 120 mm
Max pre-oxidation temperature 1290°C

200 µm

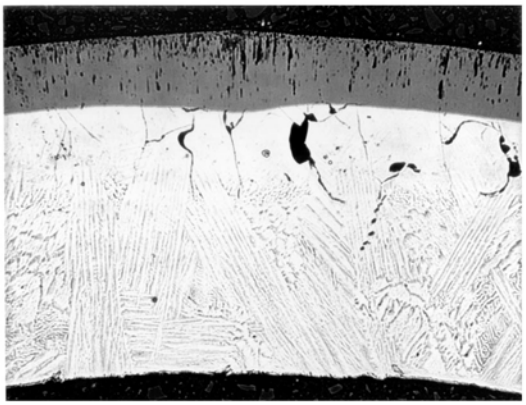

ZrO_2 152 µm
α-Zr(O) 134 µm
β-Zr 464 µm

Elevation 75 mm
Max pre-oxidation temperature 1410°C

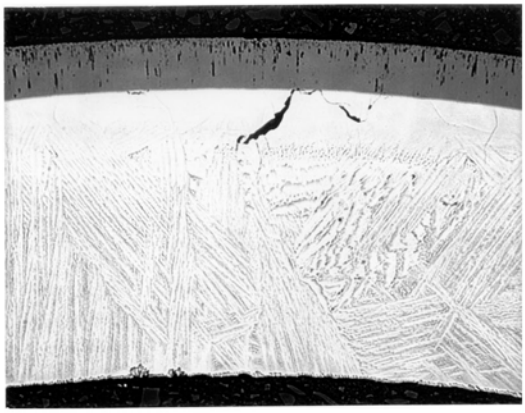

ZrO_2 113 µm
α-Zr(O) 115 µm
β-Zr 526 µm

Elevation 30 mm
Max pre-oxidation temperature 1350°C

Fig. 22: Test No. 7 (pre-oxidation period 7 min., cooldown at 1200°C). Cross sections at three TC elevations, as polished.
There are no through wall cracks

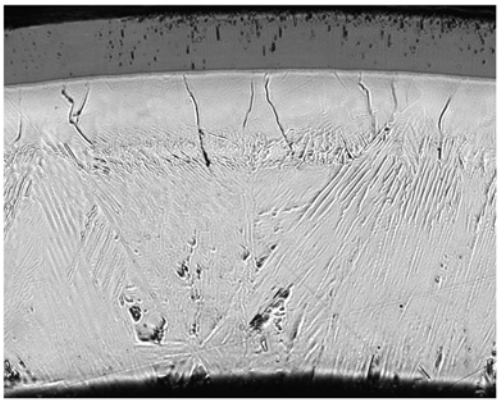

Elevation 120 mm
Max pre-oxidation temperature 1280°C

Elevation 75 mm
Max pre-oxidation temperature 1380°C

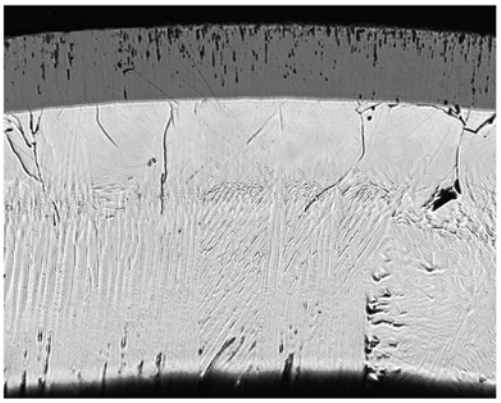

Elevation 30 mm
Max pre-oxidation temperature 1340°C

Fig. 23: Test No. 3 (pre-oxidation period 12 min., cooldown at 1200°C). Cross sections at three TC elevations, as polished.
There are no through wall cracks

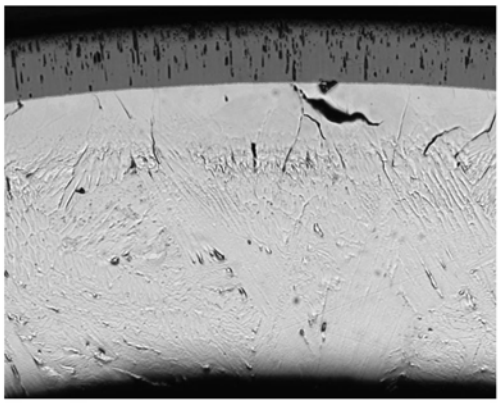

Elevation 120 mm
Max pre-oxidation temperature 1225°C

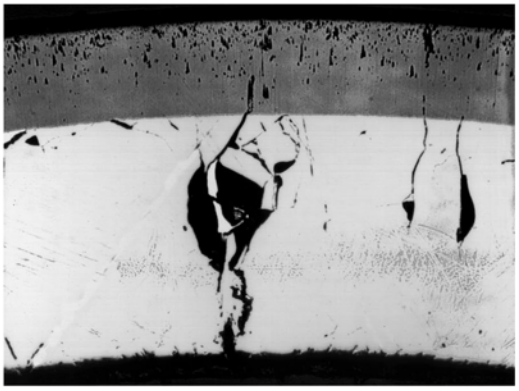

Elevation 75 mm
Max pre-oxidation temperature 1360°C

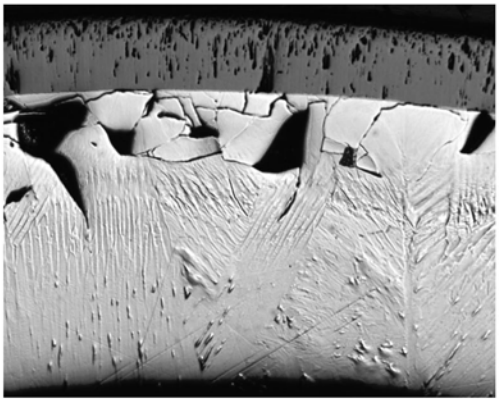

Elevation 30 mm
Max pre-oxidation temperature 1330°C

Fig. 24: Test No. 6 (pre-oxidation period 19 min., cooldown at 1200°C). Cross sections at three TC elevations, as polished.
There are a few non-oxidised through wall cracks

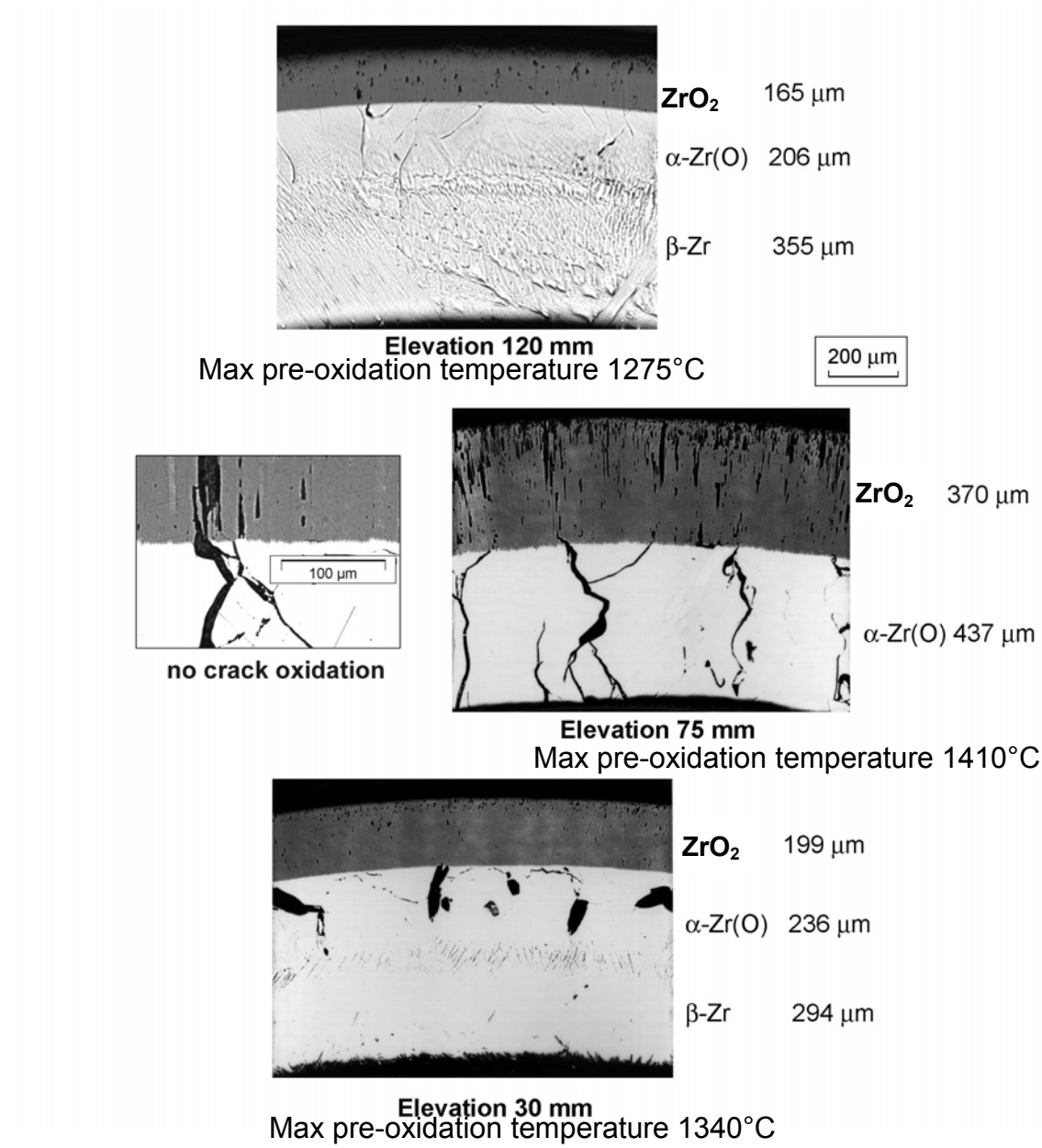

Fig. 25: Test No. 2 (pre-oxidation period 25 min., cooldown at 1200°C). Cross sections at three TC elevations, as polished.
There are few non-oxidised through wall cracks

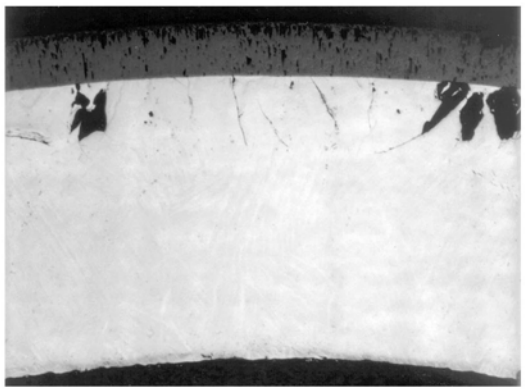

ZrO_2 121 μm

α-Zr(O) 164 μm

β-Zr 461 μm

200 μm

Elevation 120 mm
Max pre-oxidation temperature 1260°C

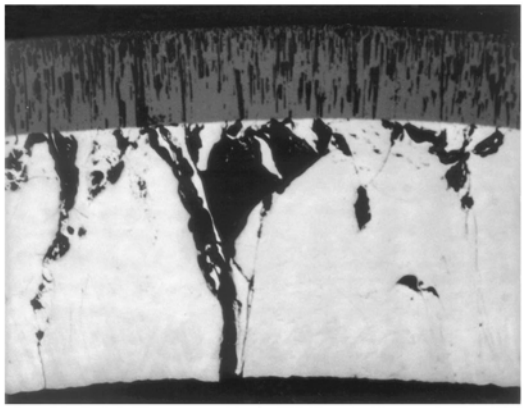

ZrO_2 207 μm

α-Zr(O) 262 μm

β-Zr 309 μm

Elevation 75 mm
Max pre-oxidation temperature 1440°C

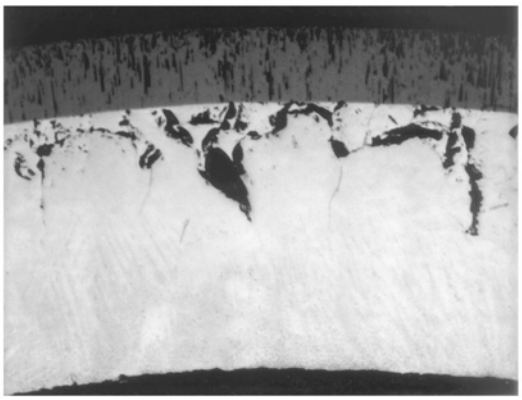

ZrO_2 167 μm

α-Zr(O) 268 μm

β-Zr 318 μm

Elevation 30 mm
Max pre-oxidation temperature 1350°C

Fig. 26: Test No. 5 (pre-oxidation period 13.5 min., cooldown at 1400°C). Cross sections at three TC elevations, as polished.
There are few not oxidised through wall cracks

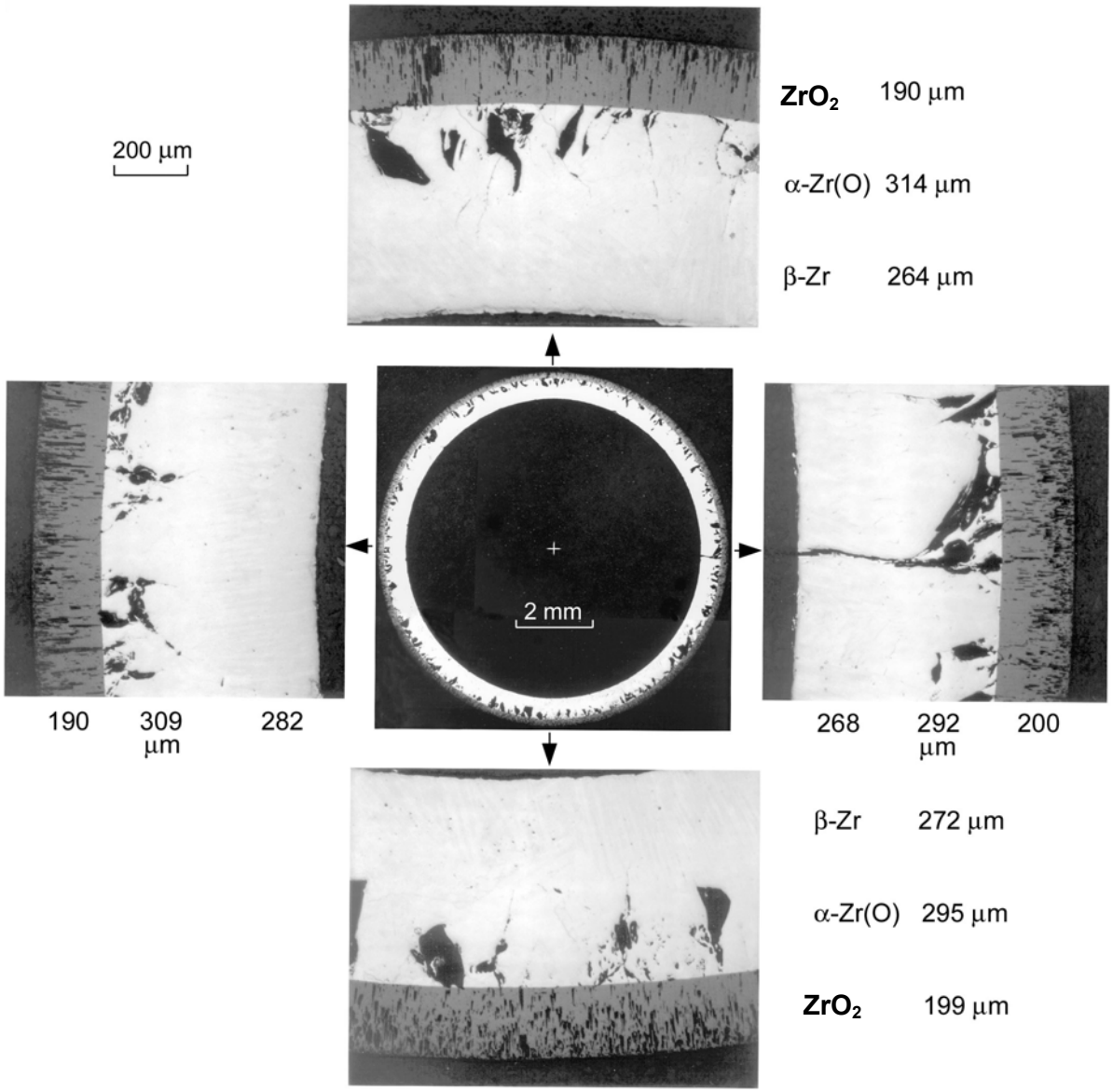

Fig. 27: Test No. 1 (pre-oxidation period 18.5 min., cooldown at 1400°C). Cross section at middle TC elevation, as polished.
There are few not oxidised through wall cracks

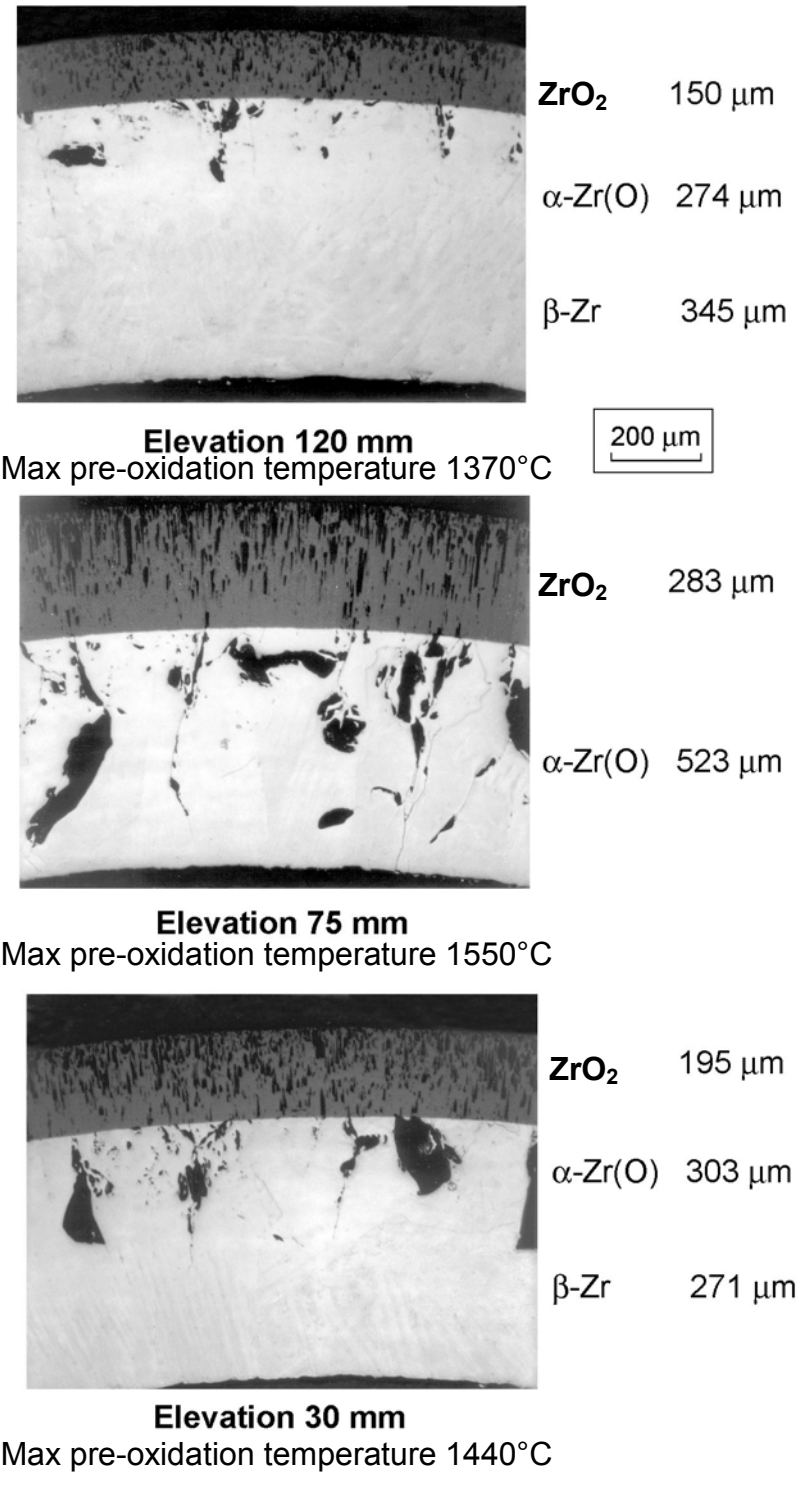

Elevation 120 mm
Max pre-oxidation temperature 1370°C

Elevation 75 mm
Max pre-oxidation temperature 1550°C

Elevation 30 mm
Max pre-oxidation temperature 1440°C

Fig. 28: Test No. 1 (pre-oxidation period 18.5 min., cooldown at 1400°C). Cross sections at three TC elevations, as polished.
There are few not oxidised through wall cracks

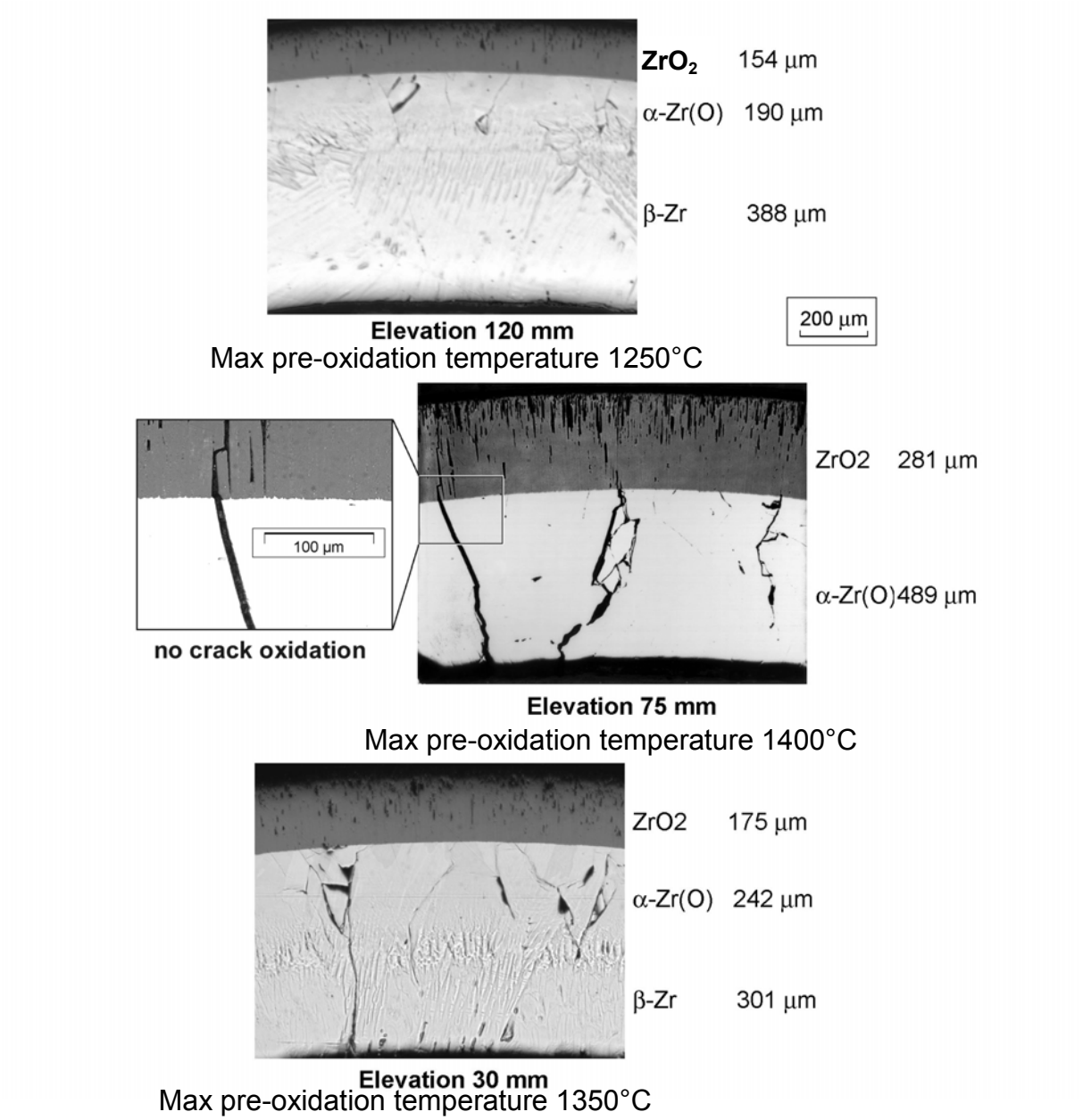

Fig. 29: Test No. 8 (pre-oxidation period 26.5 min., cooldown at 1400°C). Cross sections at three TC elevations, as polished.
There are few not oxidised through wall cracks

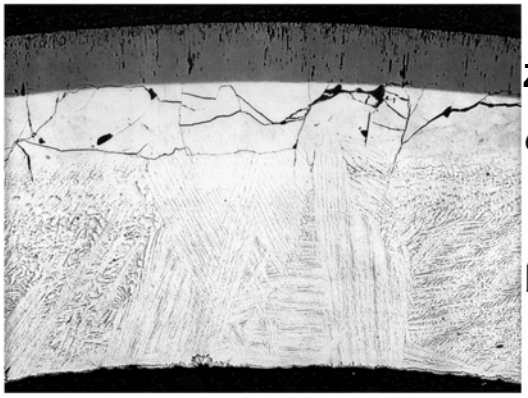

Elevation 120 mm
Quench temperature 1400°C

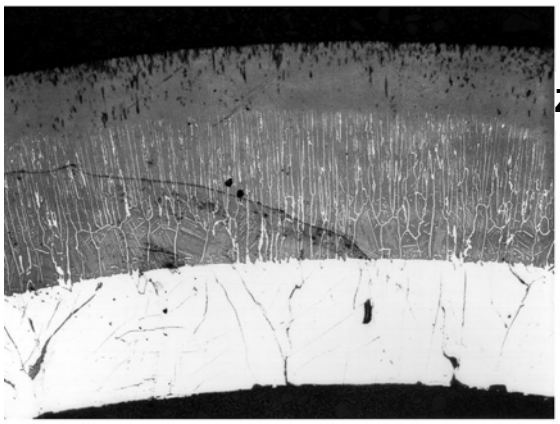

Elevation 75 mm
Quench temperature 1750°C

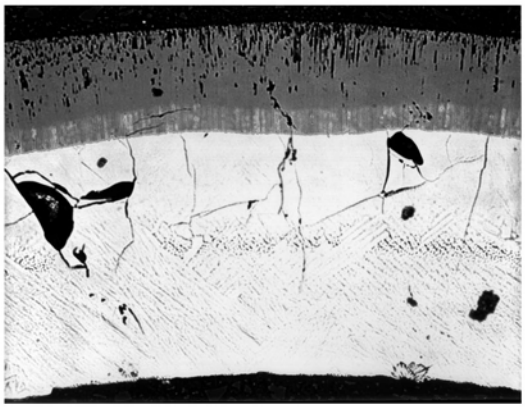

Elevation 30 mm
Quench temperature ~1600°C

Fig. 30: Test No. 4 (pre-oxidation period 6 min., cooldown at 1600°C). Cross sections at three TC elevations, as polished. The cracks are only in the □-Zr(O) layer

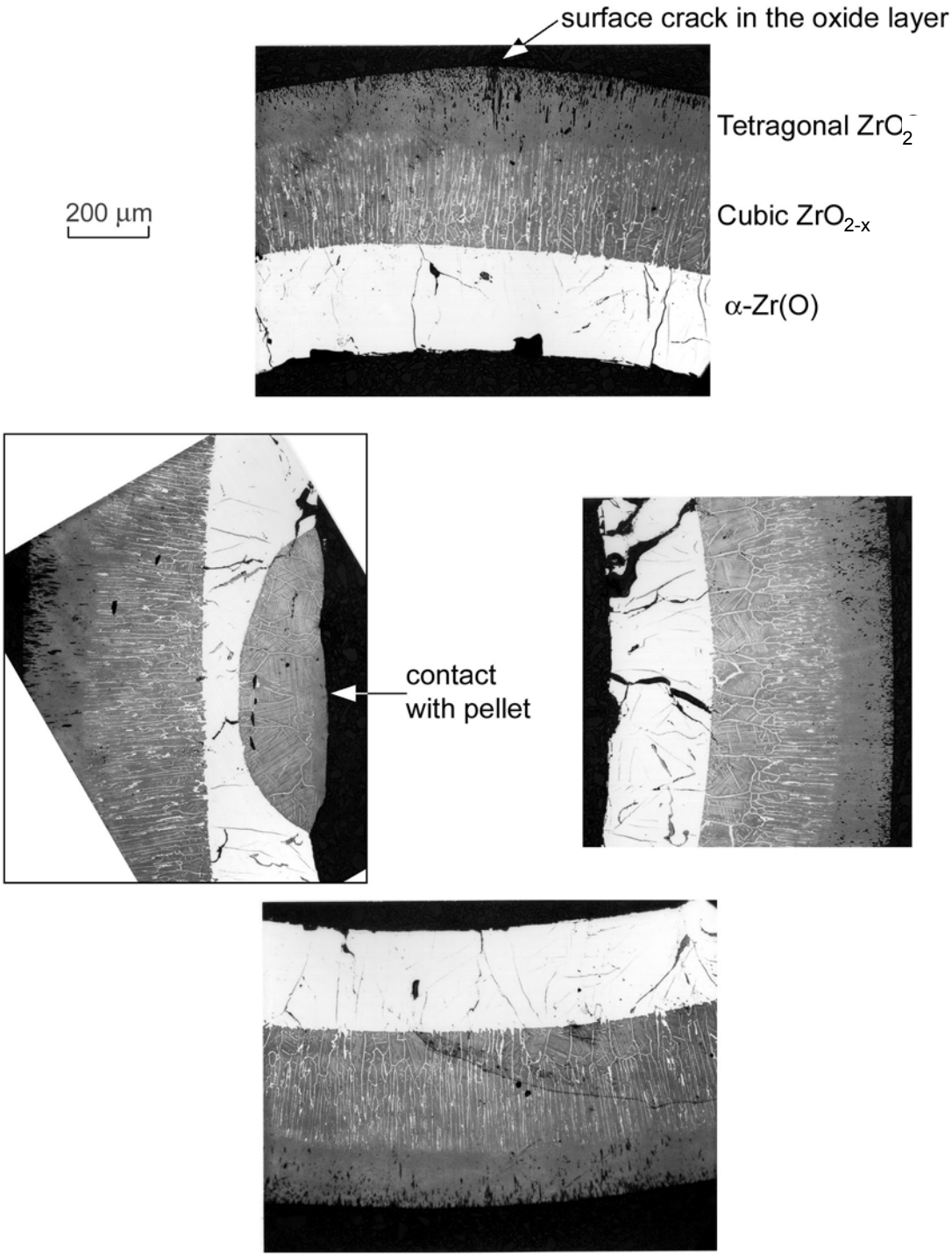

Fig. 31: Test No. 4 (pre-oxidation period 6 min., cooldown at 1600°C). Cross section at middle TC elevation, as polished

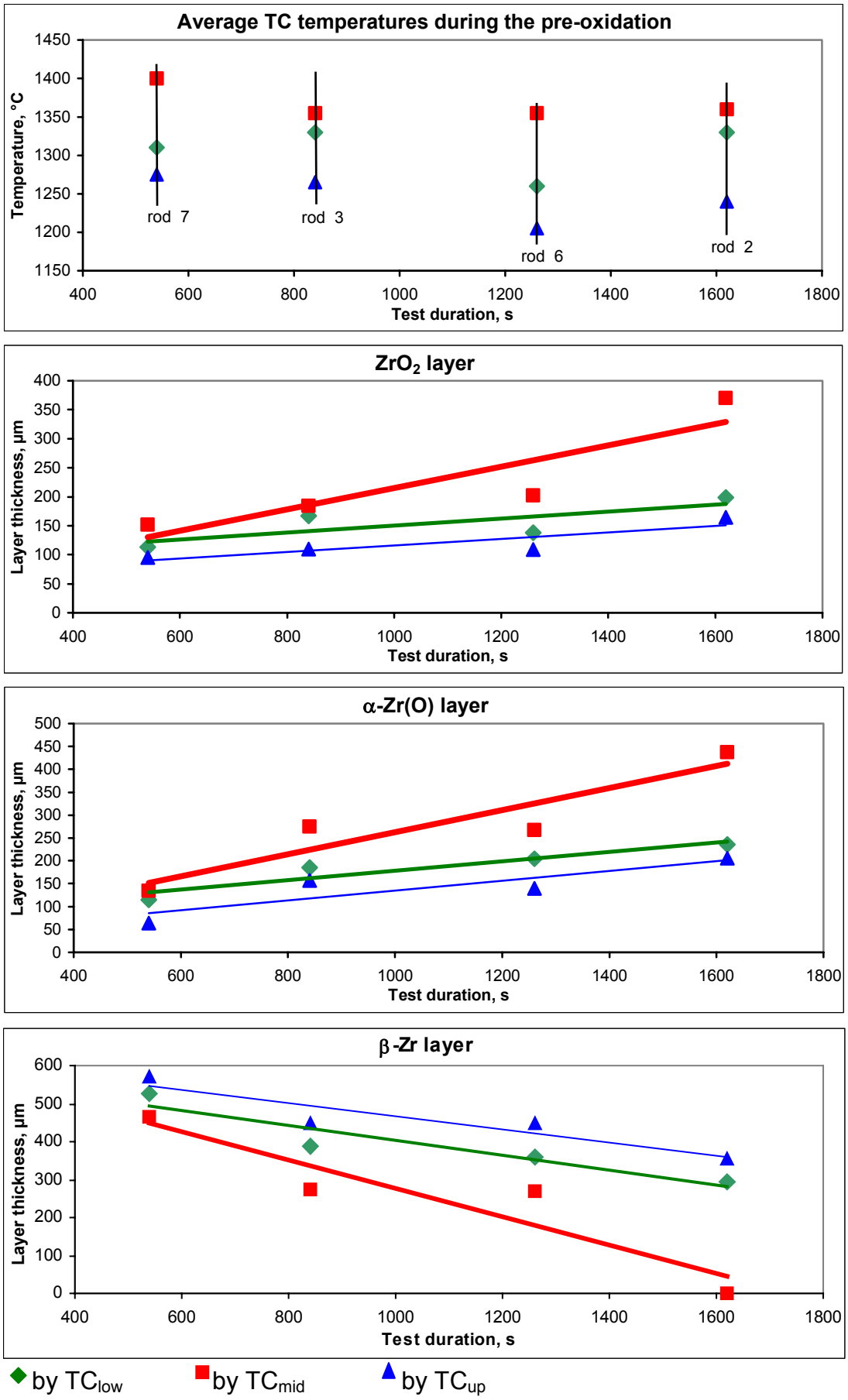

Fig. 32: Thickness of layers across a cladding after the tests with the quench temperature 1200°C

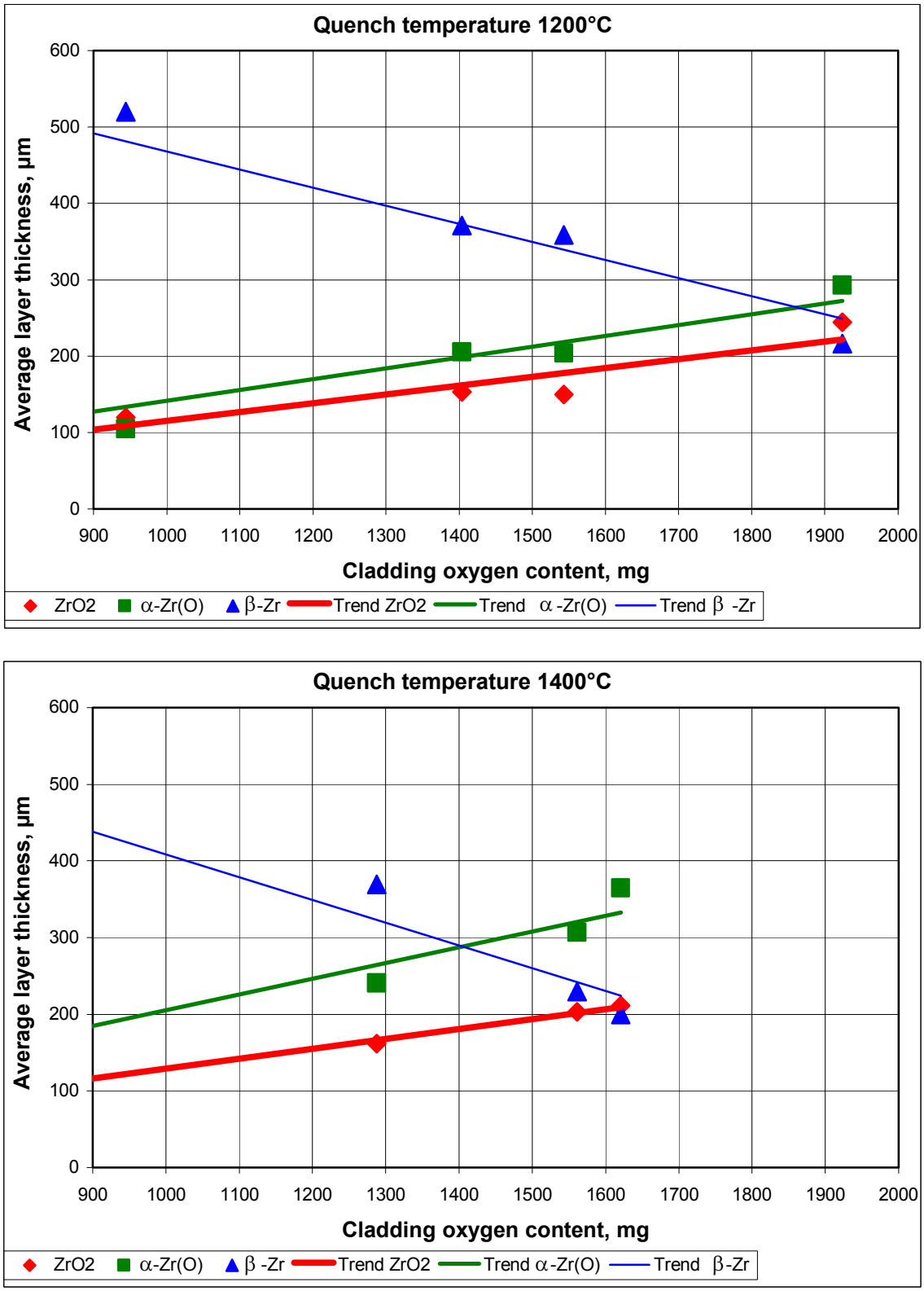

Fig. 33: Cladding layers formation depending on the cladding total oxygen content.
Oxygen content determined from the rods weight gain during the tests

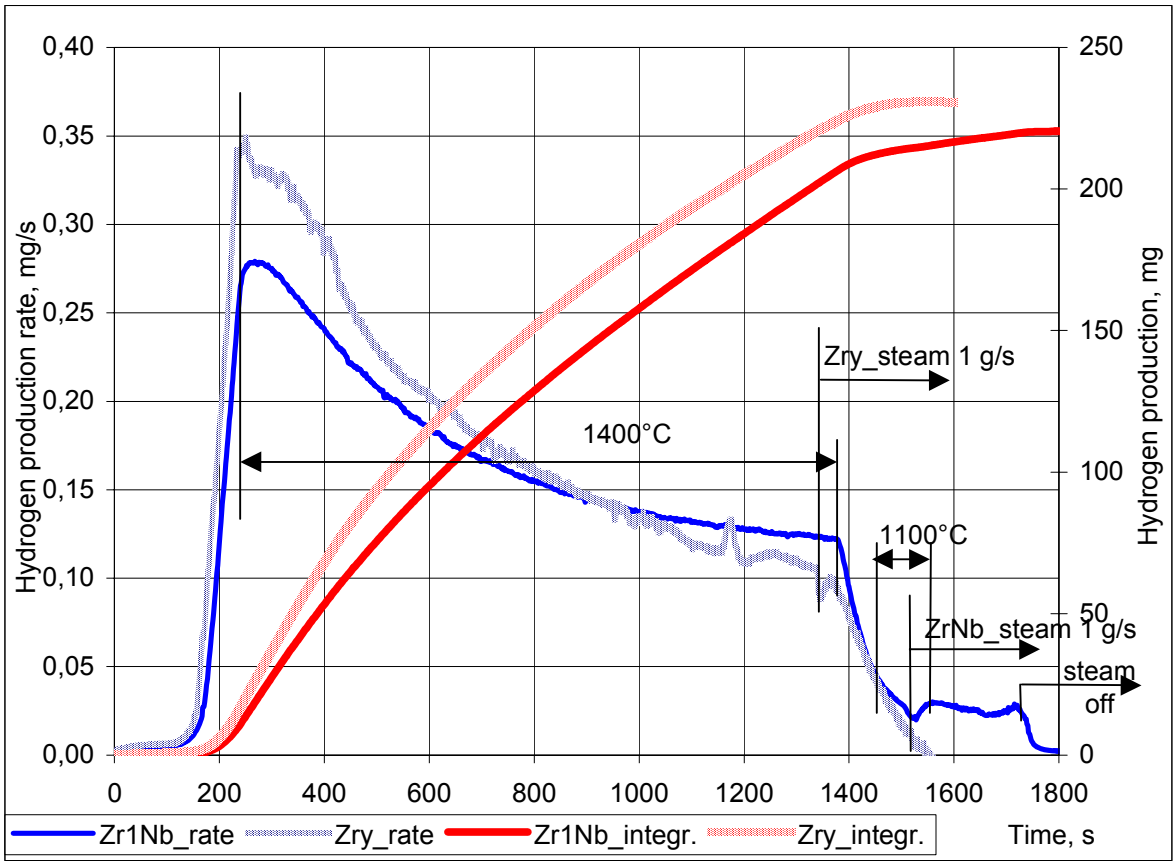

Fig. 34: Comparison of the hydrogen production for Zr-1Nb (test No.9) and Zircaloy-4 (test No. 050381) with cooldown from 1100°C

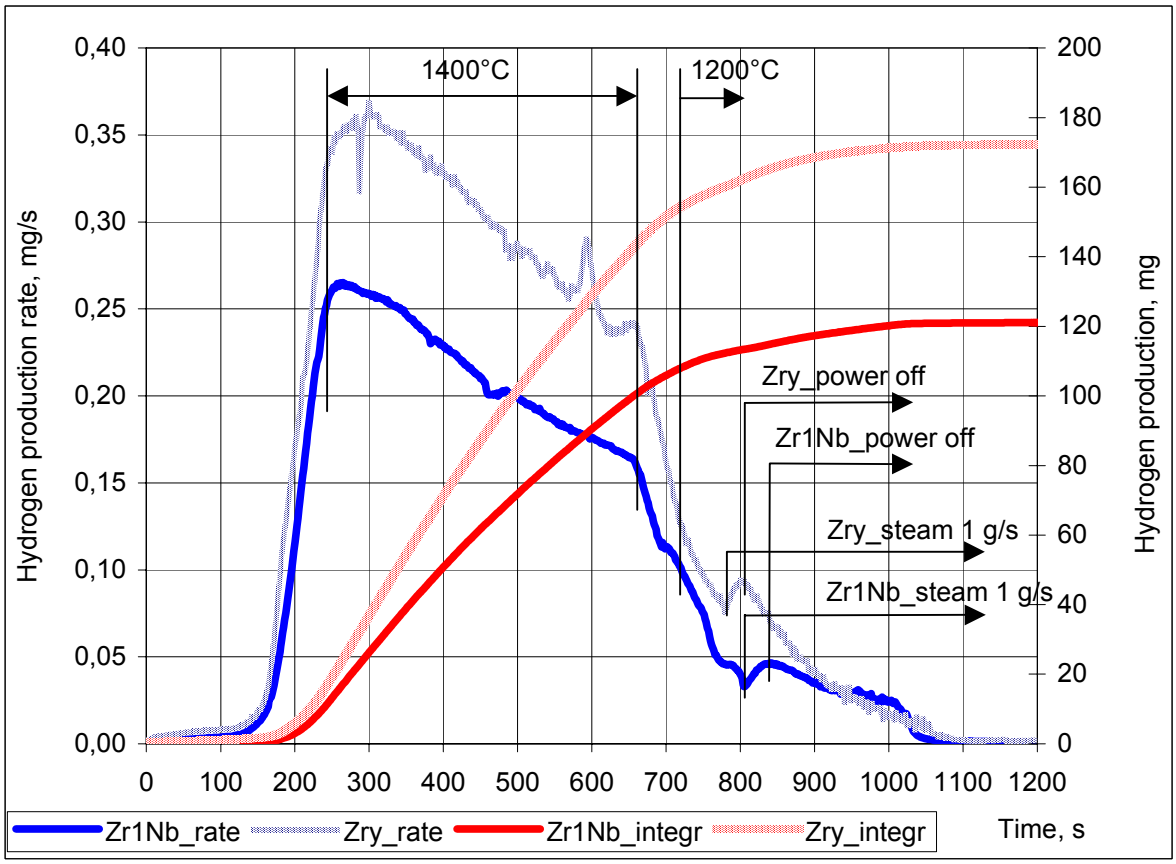

Fig. 35: Comparison of the hydrogen production for Zr-1Nb (test No.7) and Zircaloy-4 (test No. 120281) with cooldown from 1200°C

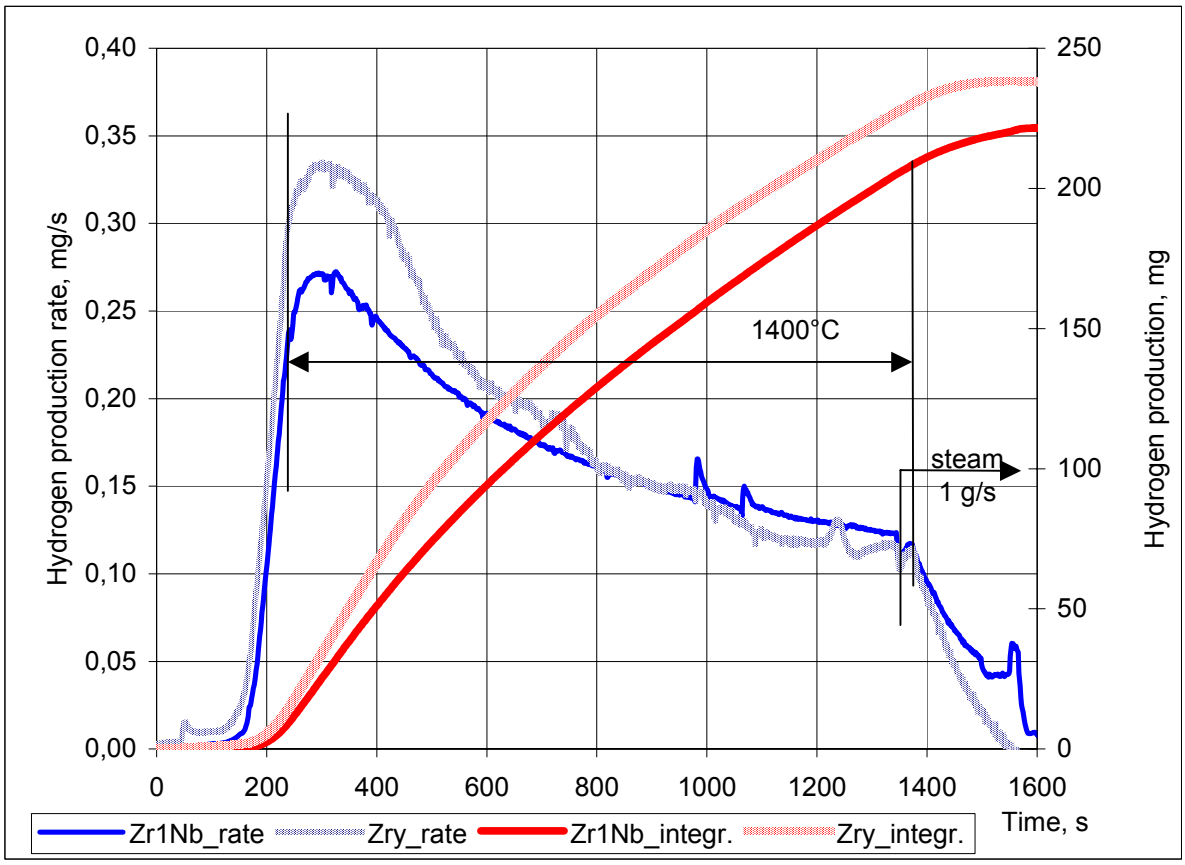

Fig. 36: Comparison of the hydrogen production for Zr-1Nb (test No.1) and Zircaloy-4 (test No. 250281) with cooldown from 1400°C

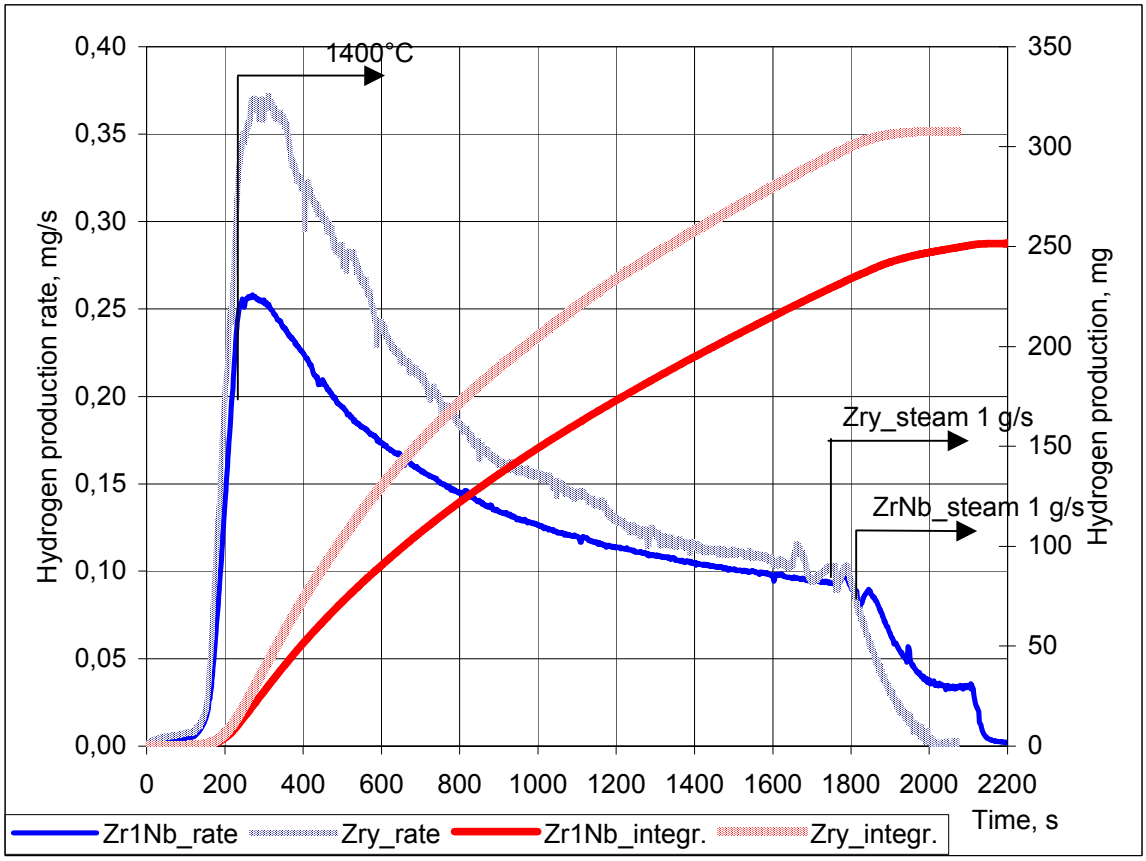

Fig. 37: Comparison of the hydrogen production for Zr-1Nb (test No.8) and Zircaloy-4 (test No. 170281) with cooldown from 1400°C

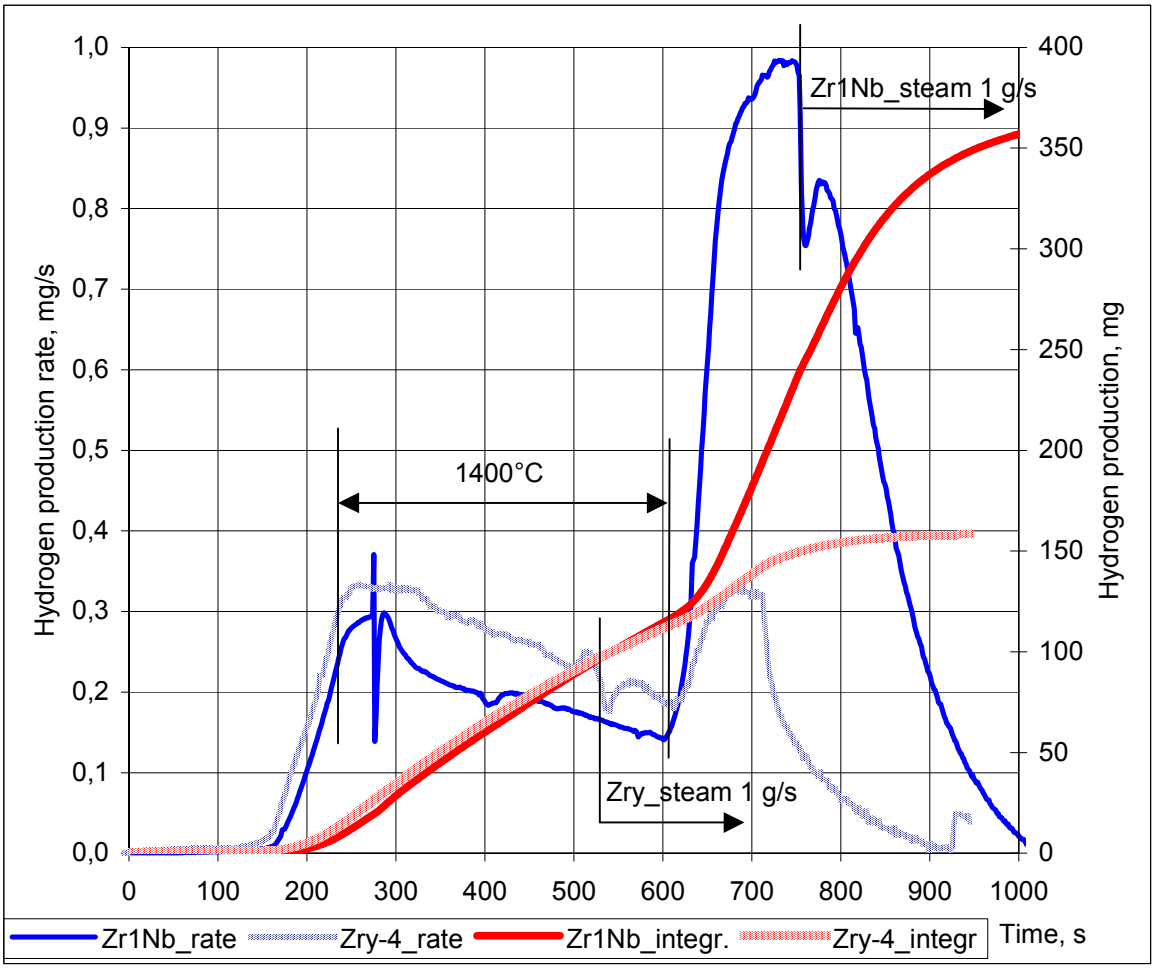

Fig. 38: Comparison of the hydrogen production for Zr-1Nb (test No.4) and Zircaloy-4 (test No. 160281) with cooldown from 1600°C

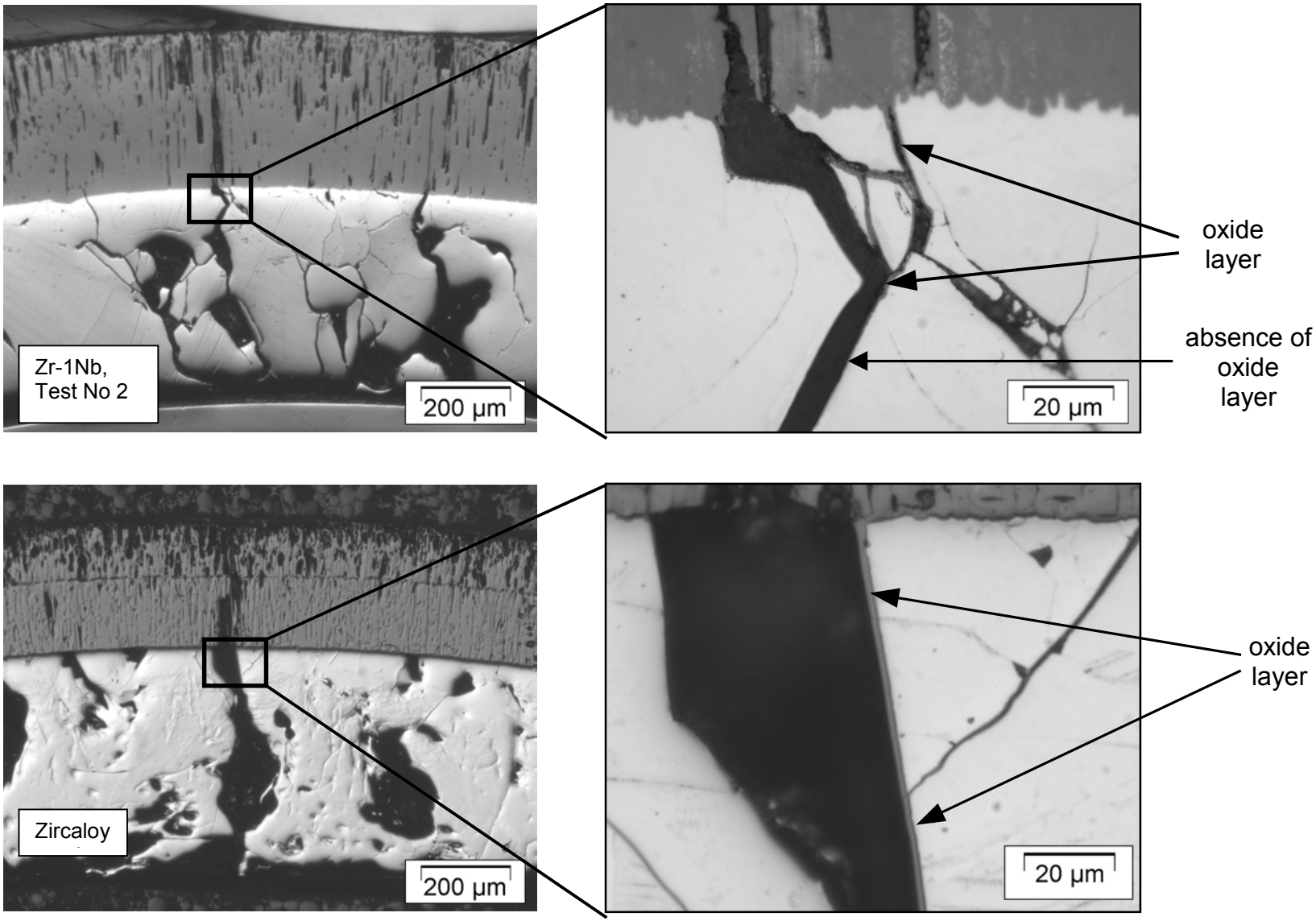

Fig. 39: Crack formation and oxidation during the steam cooldown from 1200°C. Comparison between Zr-1Nb and Zircaloy-4

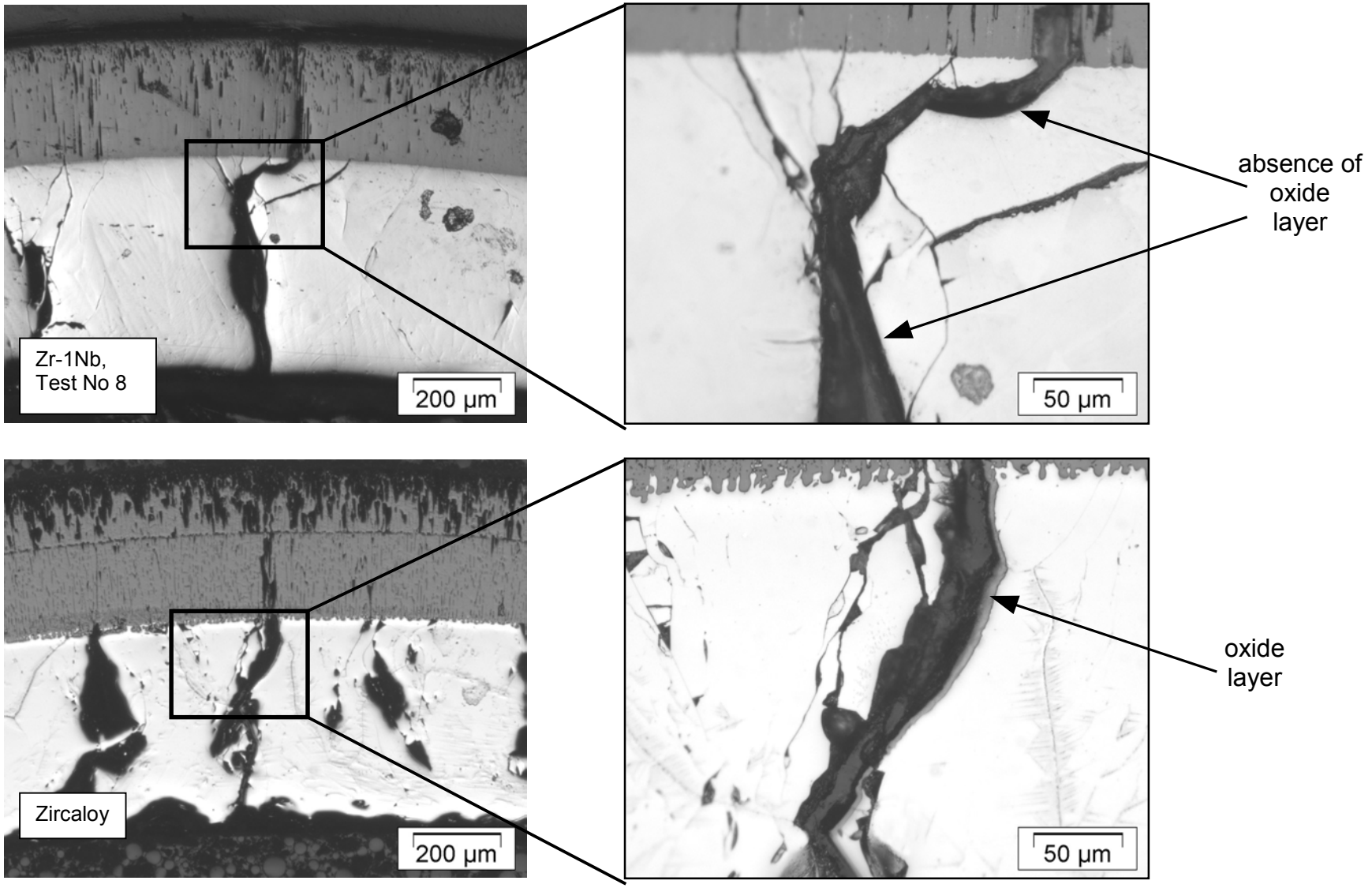

Fig. 40: Crack formation and oxidation during the steam cooldown from 1400°C. Comparison between Zr-1Nb and Zircaloy-4

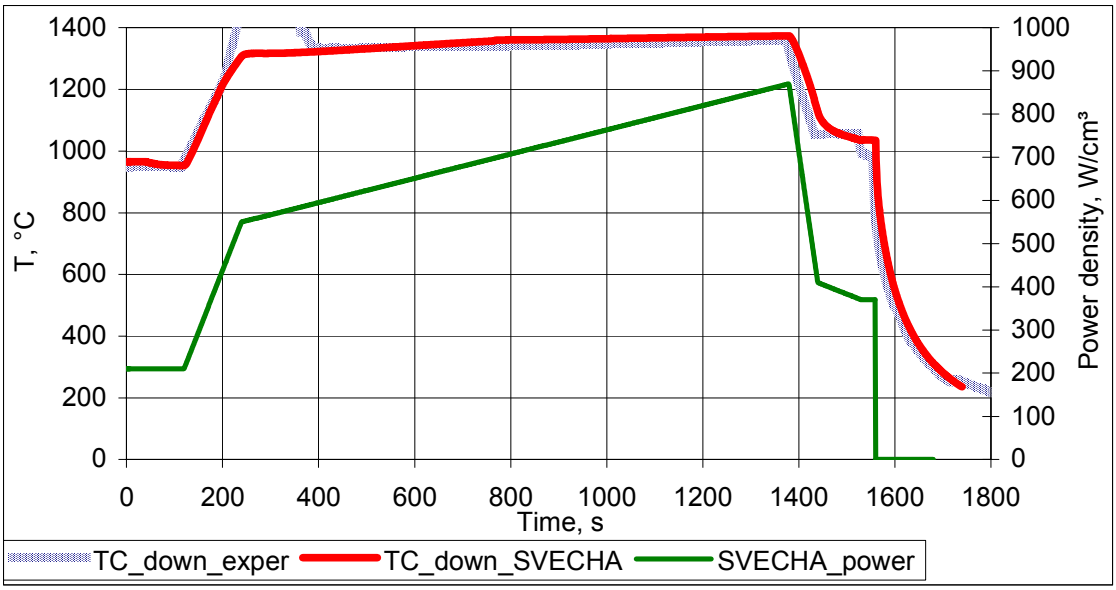

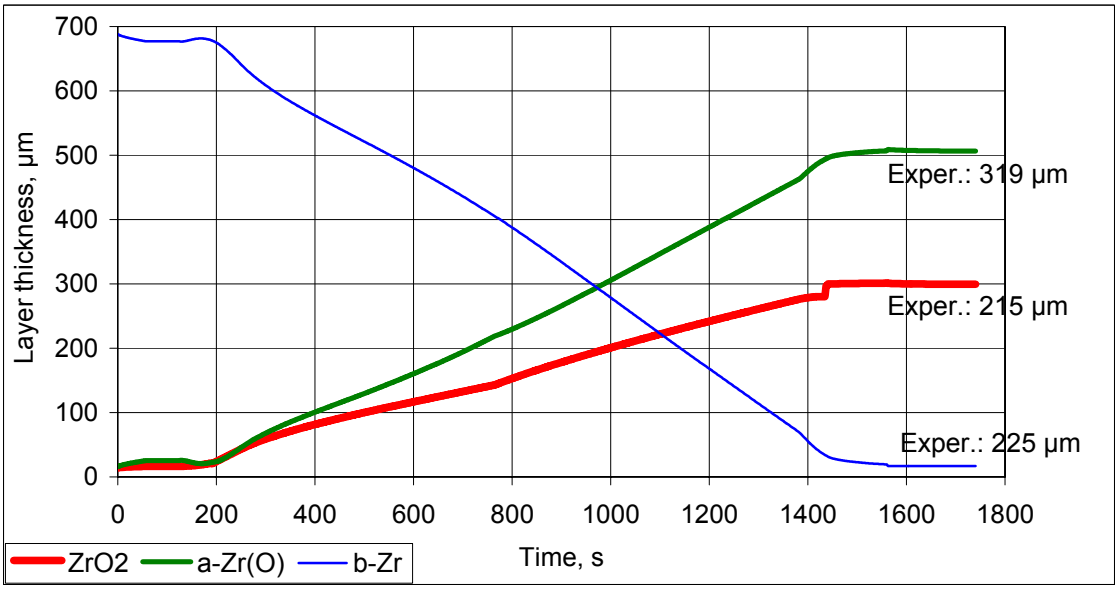

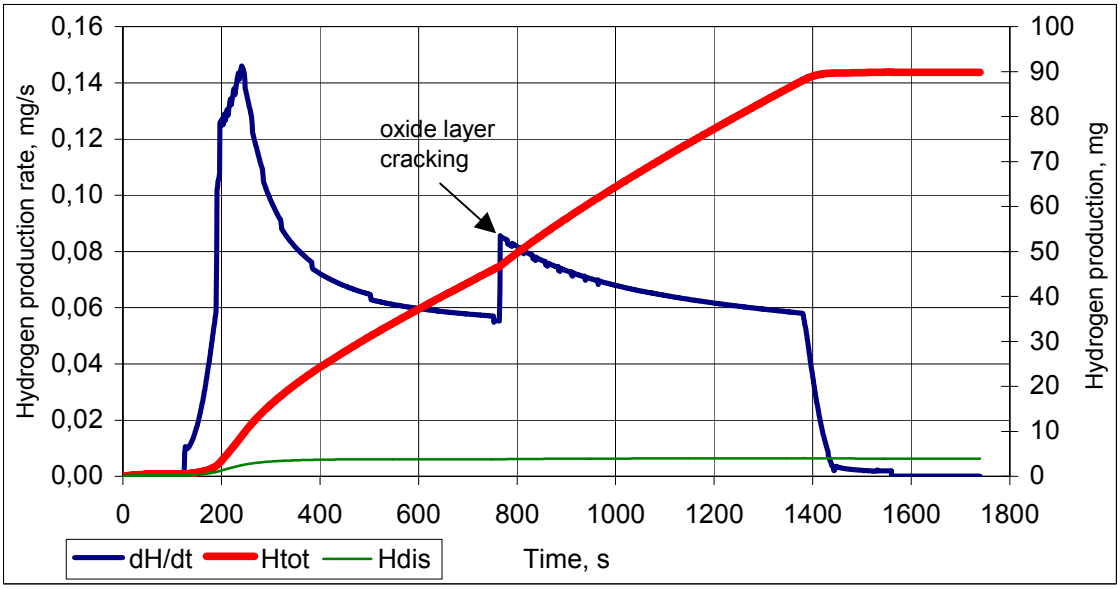

Fig. 41: SVECHA calculations for the low section (5 cm long) of rod after Test No. 9. The power is fitted according to the test temperature

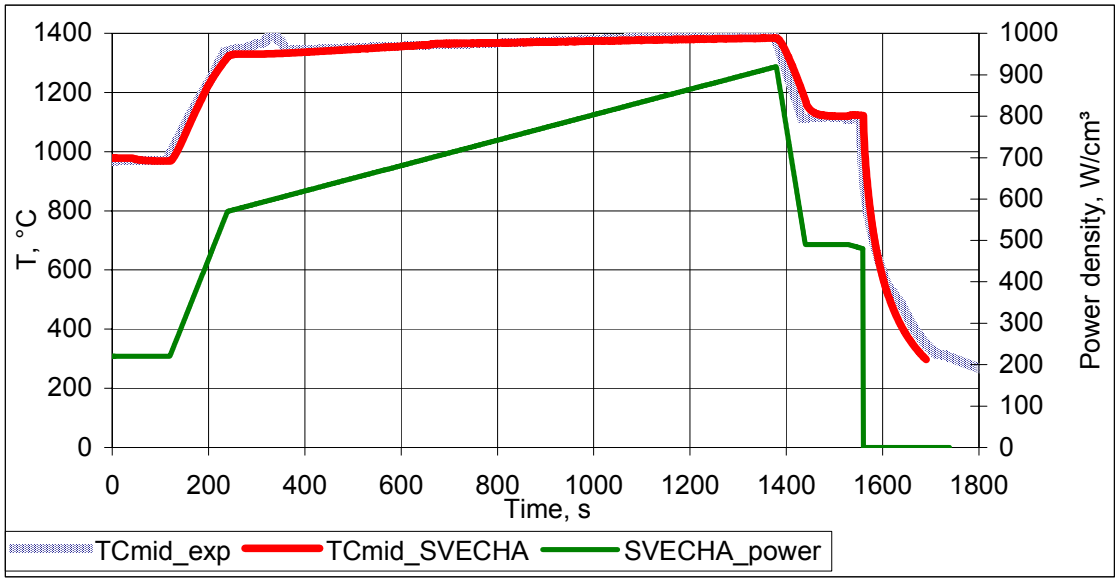

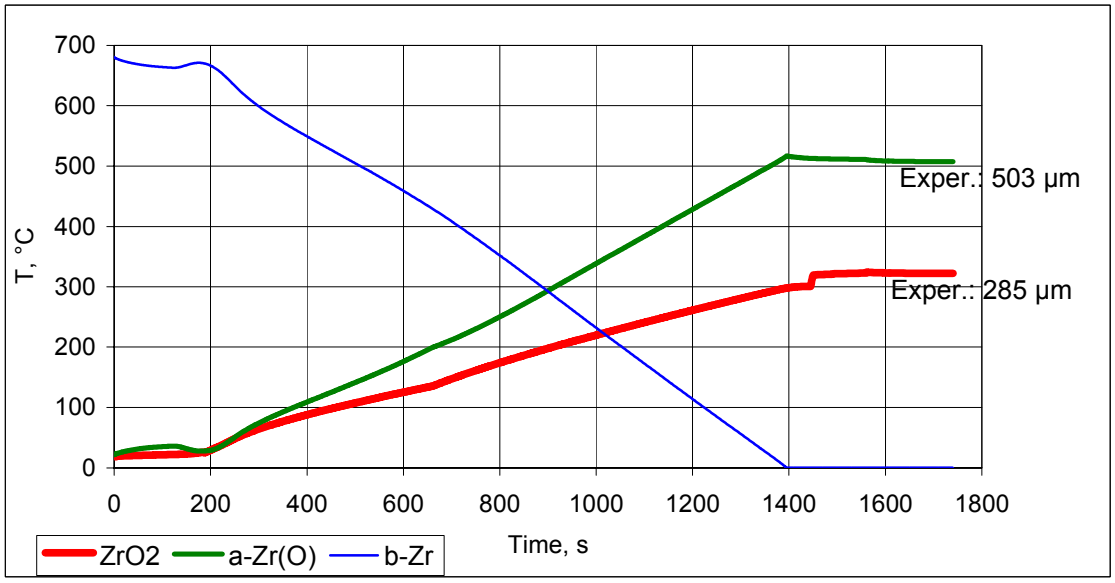

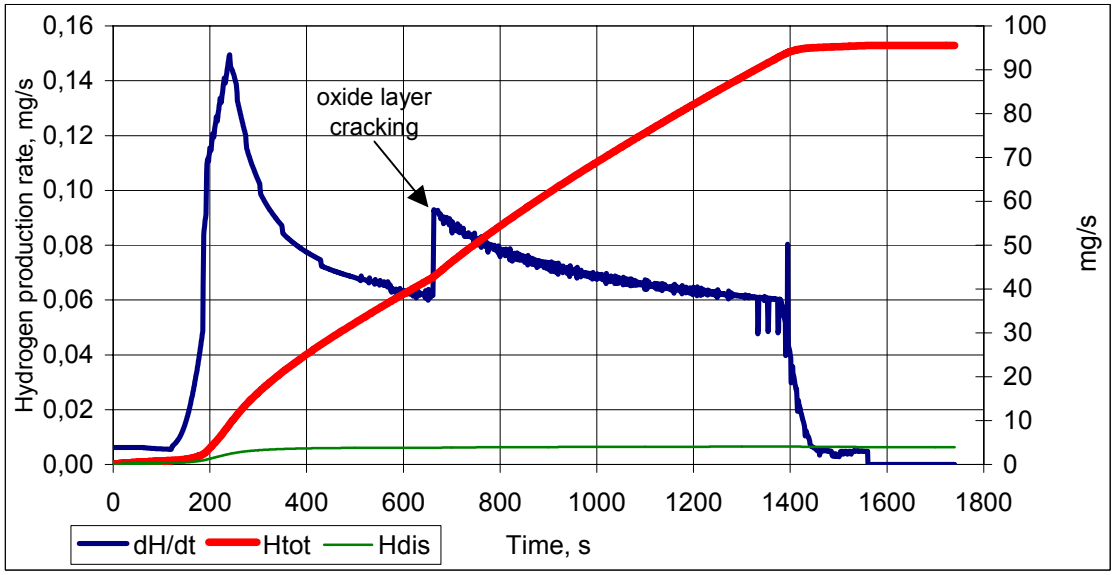

Fig. 42: SVECHA calculations for the middle section (5 cm long) of rod after Test No. 9. The power is fitted according to the test temperature profile

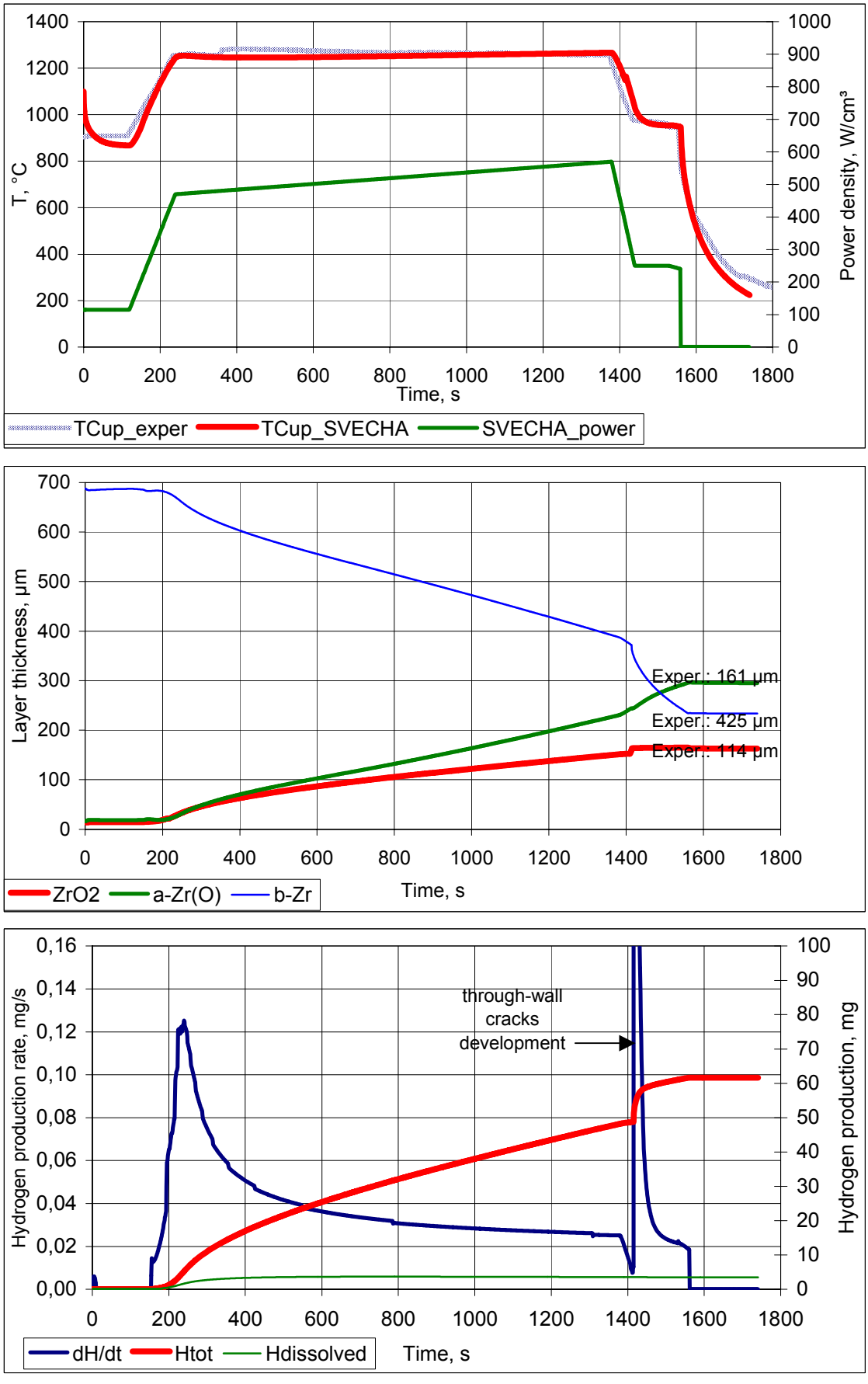

Fig. 43: SVECHA calculations for the upper section (5 cm long) of rod after Test No. 9. The power is fitted according to the test temperature profile

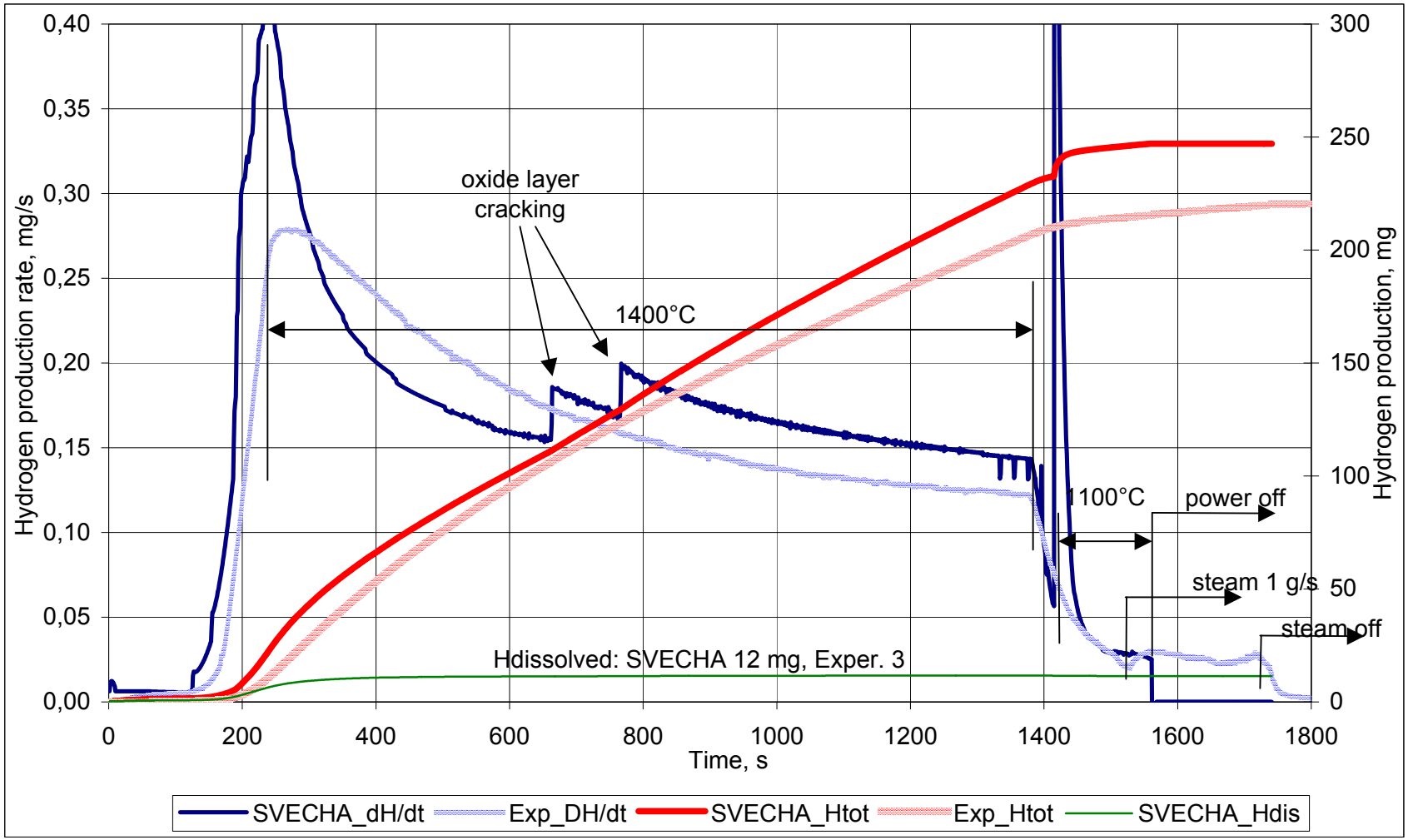

Fig. 44: Comparison of the experimental and SVECHA calculation results of the hydrogen production for the test No. 9. The hydrogen, calculated by SVECHA, is the sum of the three rod segments

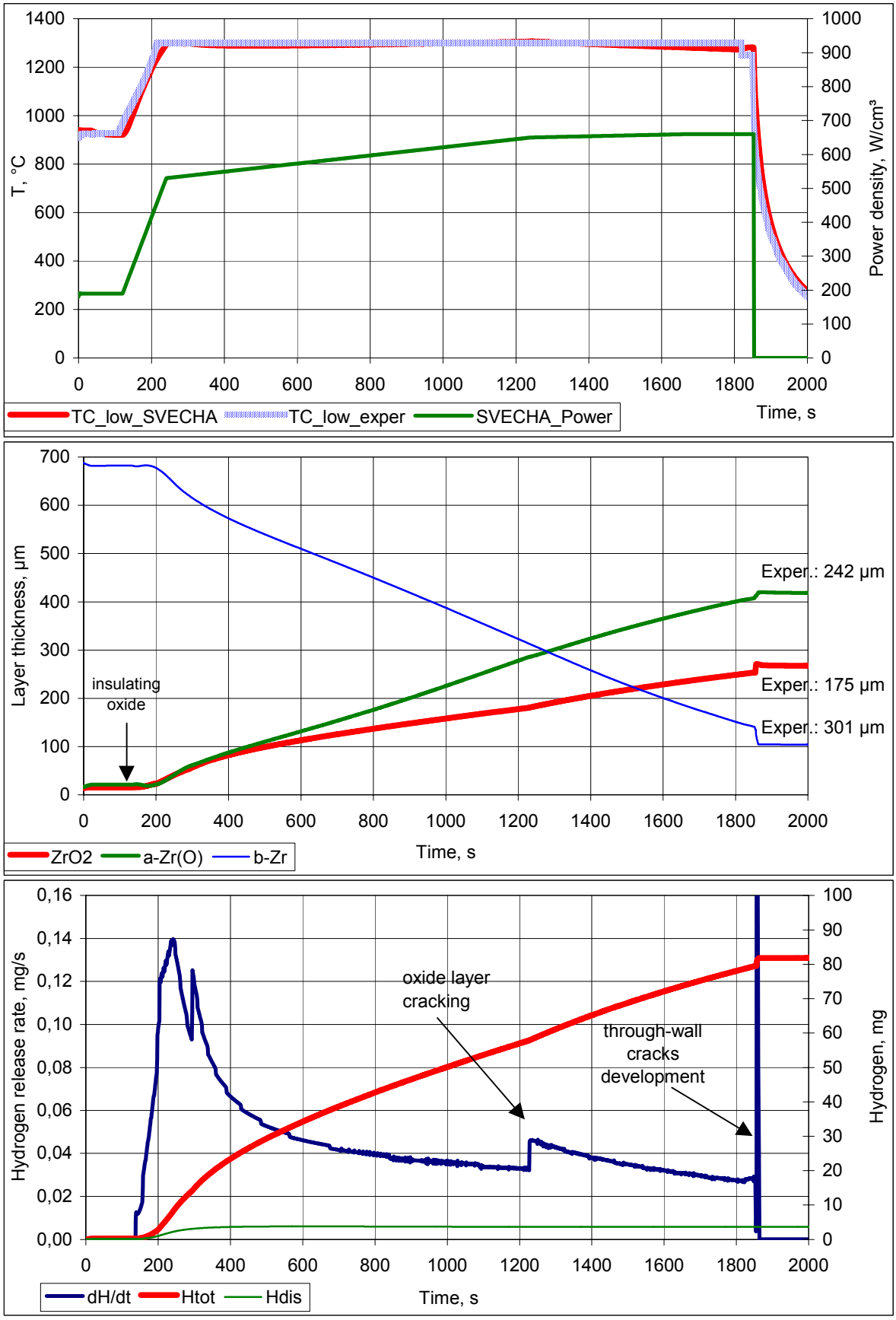

Fig. 45: SVECHA calculations for the low section (5 cm long) of rod after Test No. 8. The power is fitted according to the test temperature

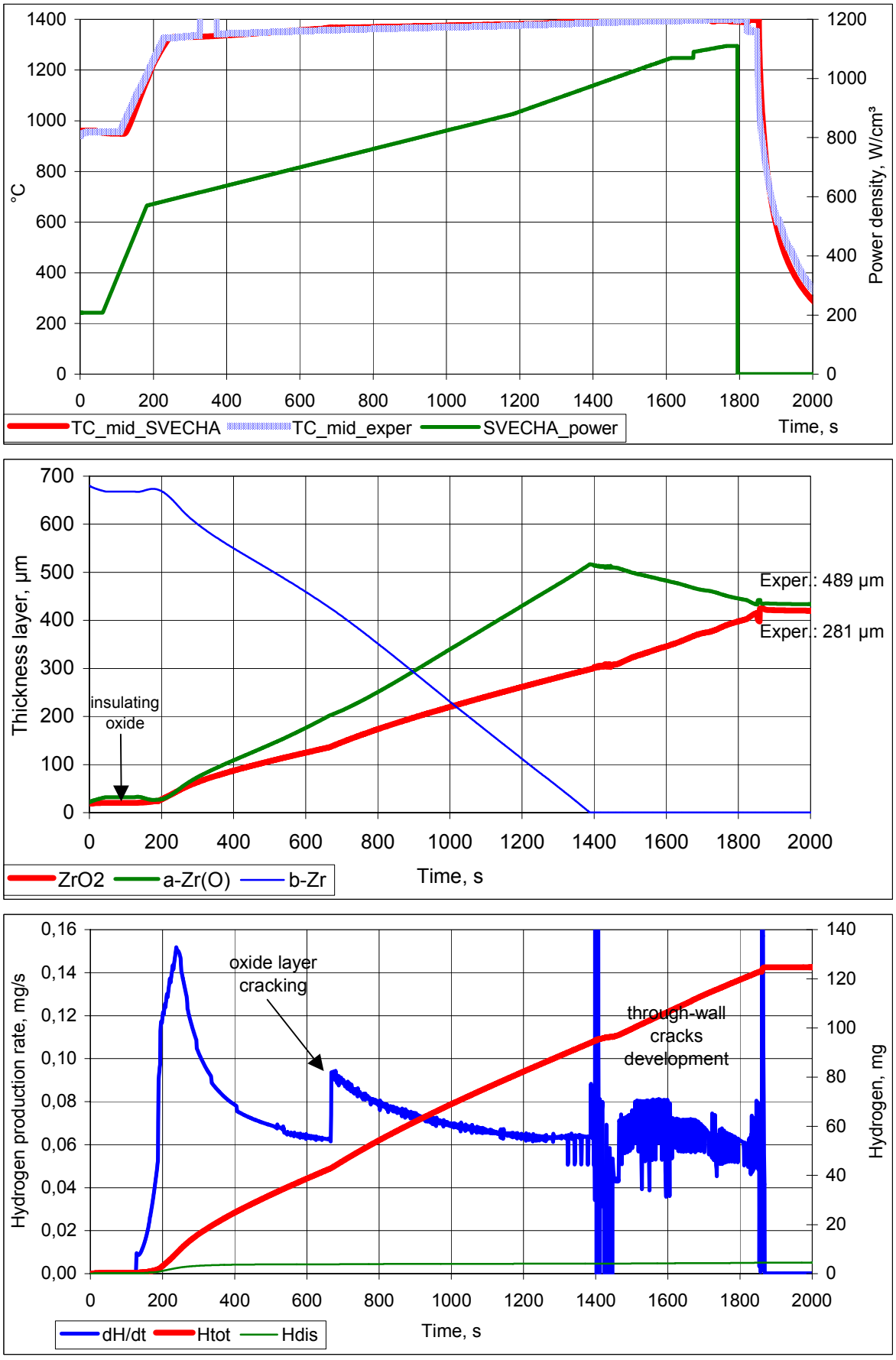

Fig. 46: SVECHA calculations for the middle section (5 cm long) of rod after Test No. 8. The power is fitted according to the test temperature profile

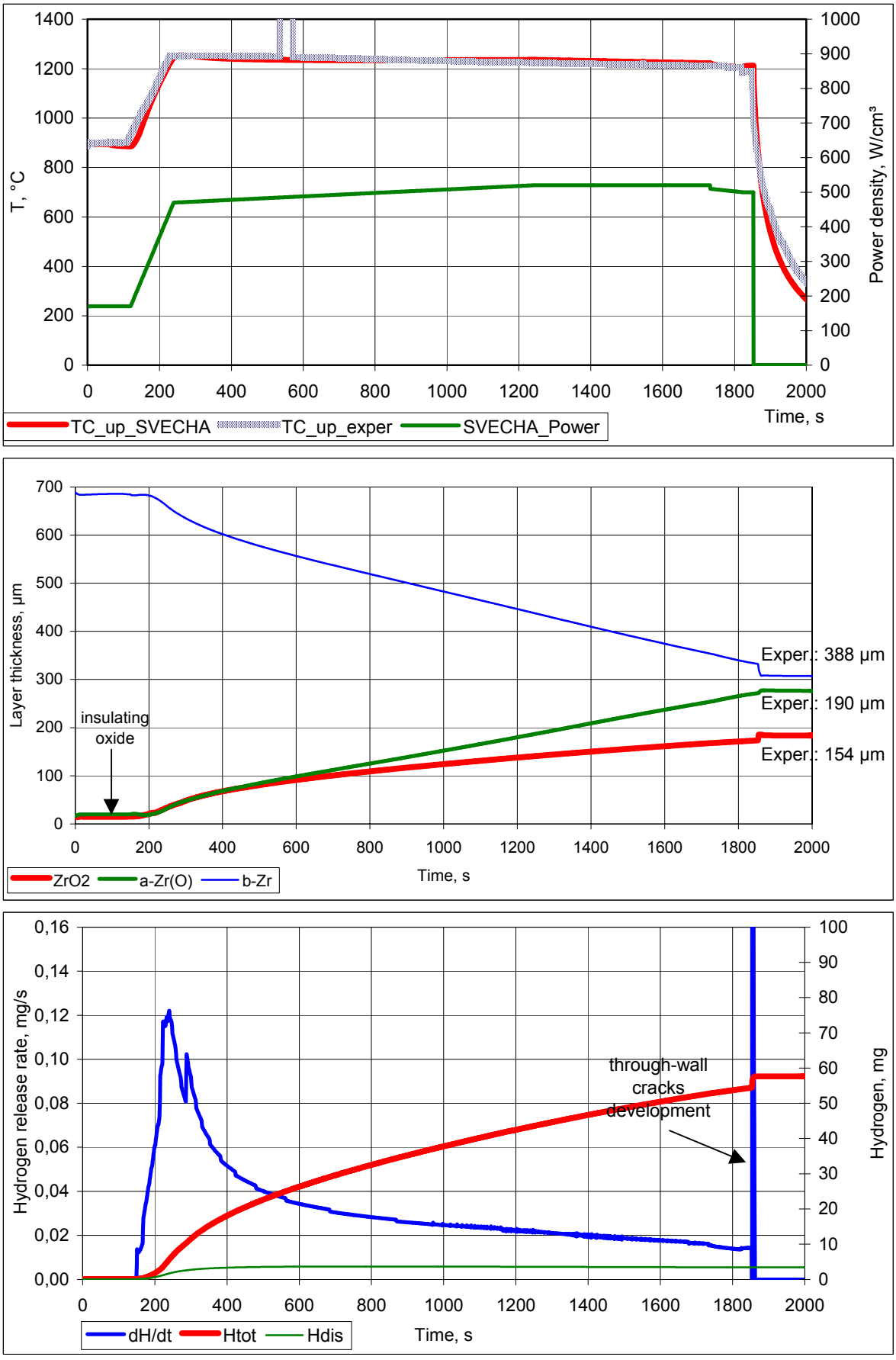

Fig. 47: SVECHA calculations for the upper section (5 cm long) of rod after Test No. 8. The power is fitted according to the test temperature profile

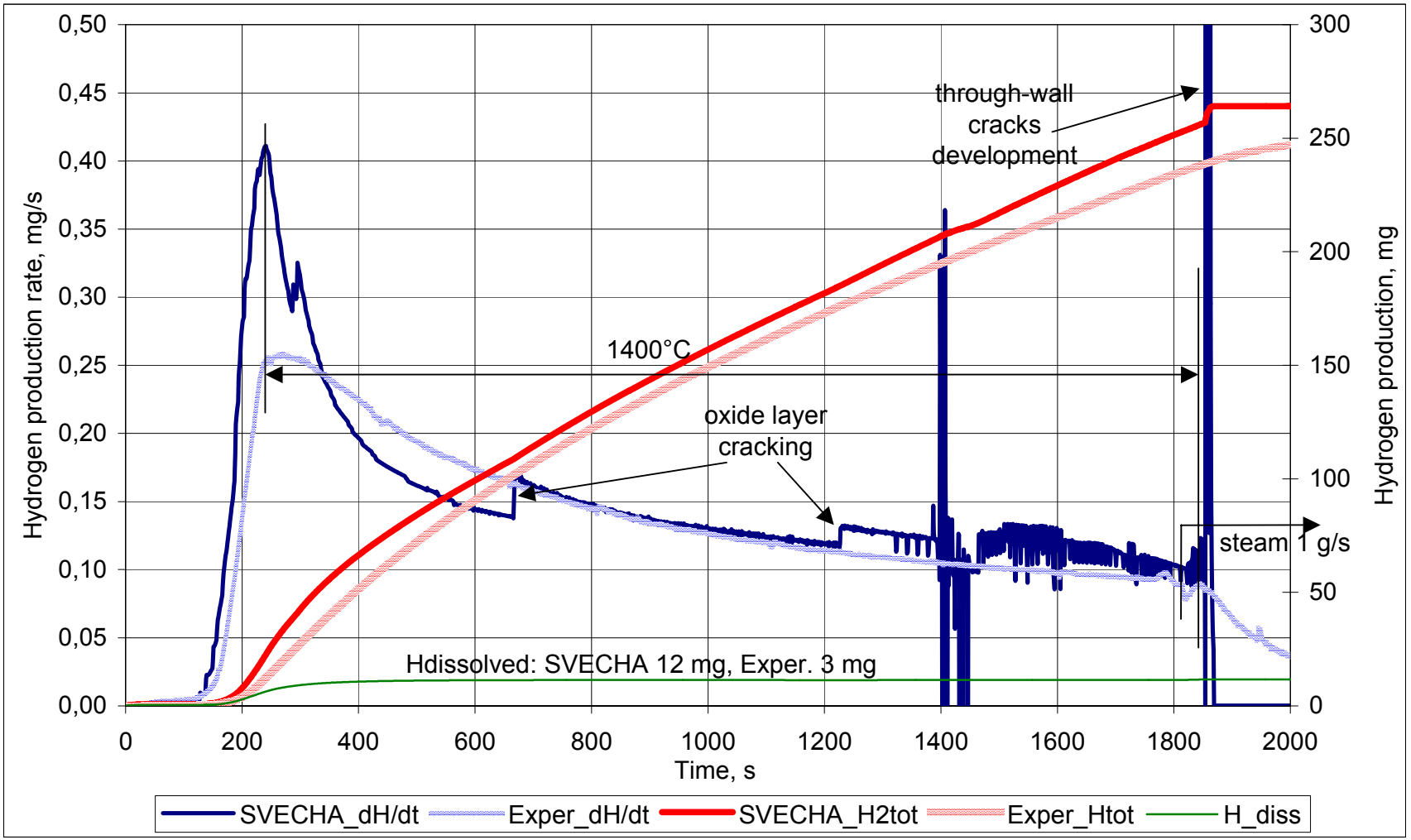

Fig. 48: Comparison of the experimental and SVECHA calculation results of the hydrogen production for the test No. 8. The SVECHA hydrogen is the sum of the three rod segments